GAMMA RAY SCATTERING WITHIN THIN-WALLED SHELLS

by

William Bartow Wolfe

A Thesis Submitted to the
Graduate Faculty in Partial Fulfillment of
The Requirements for the Degree of
MASTER OF SCIENCE

Major Subject: Nuclear Engineering

Approved:

Iowa State College
1957

TABLE OF CONTENTS

I. INTRODUCTION

A major problem associated with the present development of nuclear power and the widespread use of radioisotopes is that of providing protection for human beings against gamma radiation. To provide adequate shielding which completely surrounds a source of intense gamma activity is usually an expensive undertaking, requiring materials which are very heavy or very bulky or both.

An alternative to the full shield is a partial or shadow shield placed between the personnel and the radioactive source which will absorb the direct radiation. Such a shield type may be employed to advantage in nuclear powered aircraft, nuclear powered ships or submarines, storage tanks for spent fuel elements or other applications where limited access by personnel obviates the need for a shield which completely surrounds the source of radiation.

However, the use of a shadow shield to block the direct radiation leaves the problem of the gamma rays which are scattered around and over the shadow shield by the material in the surrounding structure. Thus, it becomes important in the design of shielding systems to be able to predict the amount of gamma activity scattered into a given region by the adjacent structure such as an aircraft fuselage, a bulkhead or a storage tank wall.

In 1955, Kenneth C. Ney (1), in his thesis for the Master of Science degree, reported his study of gamma rays scattered by thin-walled cylindrical shells. The object of the study treating both gamma rays and neutrons was to establish the relationship between the scattering in a model of an airplane fuselage and the scattering in a full-scale structure. A theoretical analysis was made of the scattering in a cylindrical geometry, and an experimental study was conducted to verify the theoretical analysis. Although the findings indicated similar trends in both the theoretical and experimental work, the results for various reasons were not conclusive.

The purpose of the present study is twofold. The first objective is to re-examine the theoretical analysis of the scattering problem and make the necessary modifications in order to achieve a more useful expression for the scattering of photons in a cylindrical geometry. The second objective is to conduct an experimental study in an attempt to eliminate the difficulties of the previous investigator and thereby obtain a means of verifying the theoretical analysis.

II. SCOPE OF INVESTIGATION

Before elaborating on the present investigation, it is important to define the specific problem under study and outline the investigation that has previously been made of this subject.

A point source of isotropic gamma radiation is located on the longitudinal axis of a cylindrical shell. Of the photons that arrive at the shell wall, a certain portion pass through the wall unaffected, some are completely absorbed in the wall, and some are scattered by the wall and emerge with increased wavelength in a new direction. The specific problem is to determine what portion of the photons emitted by the point source are scattered by the shell wall into a finite target located also on the cylinder axis.

With the exception of the thesis by Ney, no literature was found on the subject of geometrical considerations in gamma ray scattering in thin absorbers. Considerable investigation has been made of gamma scattering in infinite and semi-infinite media, but since such treatments are not directly applicable to the problem at hand, a review of this literature is considered unnecessary here.

In Ney's investigation, a theoretical analysis was made of the scattering in the shell wall as a function of source strength, scattering cross sections, shell materials and other geometrical parameters. An equation was developed

for finding the activity scattered into a cylindrical target representing a detector tube. With some simplifying assumptions the equation was solved for a variety of wall thicknesses, shell radii and source-to-detector distances. Then experiments were conducted to verify the analytical findings. Although the experimental results indicated the same trends predicted by the theory, the statistical uncertainties in the experimental data were so great that the findings were not conclusive. Ney attributed the large statistical deviations to the scattering of gamma rays by the air and walls of the room, which made a large contribution to the counting rates as compared to the shell scattered activity.

The emphasis of the present study is focused on (1) analyzing the approach of the previous investigator; (2) locating the areas, both theoretical and experimental, where weaknesses or difficulties existed, and (3) eliminating these weaknesses and difficulties in order to achieve a useful theoretical expression for thin-wall gamma scattering which can be verified by experiment.

In the present study, as in the previous one, the principles of gamma ray interactions with matter are applied to the problem in order to obtain an expression for the activity scattered into a small cylindrical detector by a thin-walled shell. The investigation is restricted to photons within the energy range of a few Mev. The scattering material of the shell wall is restricted to materials of

low atomic number. These restrictions confine the problem to one primary type of interaction, Compton scattering, which for light elements comprises essentially the entire absorption coefficient for gamma rays between 0.5 and 5 Mev.

After the theoretical expression is simplified and the simplifying assumptions justified, the expression is solved by a direct analytical method and also by a graphical method. The graphical method has the advantage of treating several nearly-constant terms as variables which, in the analytical method, must be treated as constants in order for the expression to be analytically integrable.

Finally, an experimental study has been conducted to verify the theory. Employing a similar source, detector and geometrical arrangement, the experiments are essentially the same as those conducted by Ney, although more shells and shell parameters are measured. Here, the difficulties encountered in the previous work are eliminated and, consequently, the resultant data are conclusive.

III. ANALYSIS

A. Development of the Theoretical Equation

1. Application of principles

The method of developing the desired theoretical equation consists of determining the proper scattering expression for a small differential volume in the shell wall as a function of all the contributing variables, and then integrating this differential expression through the entire volume of the shell to obtain the total activity scattered into the target. Illustrated in Figure 1 is the gamma ray scattering geometry. One quarter of the cylindrical shell is shown with the source and the cylindrical detector located on the axis of the shell.

The dimensions and angles used in the development are labeled on the sketch. The other terms are defined as follows:

Symbol	Units	Definition
S	$\frac{\text{photons}}{\text{second}}$	Source strength
μ_a	cm^{-1}	Total absorption coefficient for gamma rays in air.
μ_w	cm^{-1}	Total absorption coefficient for gamma rays in the shell wall.

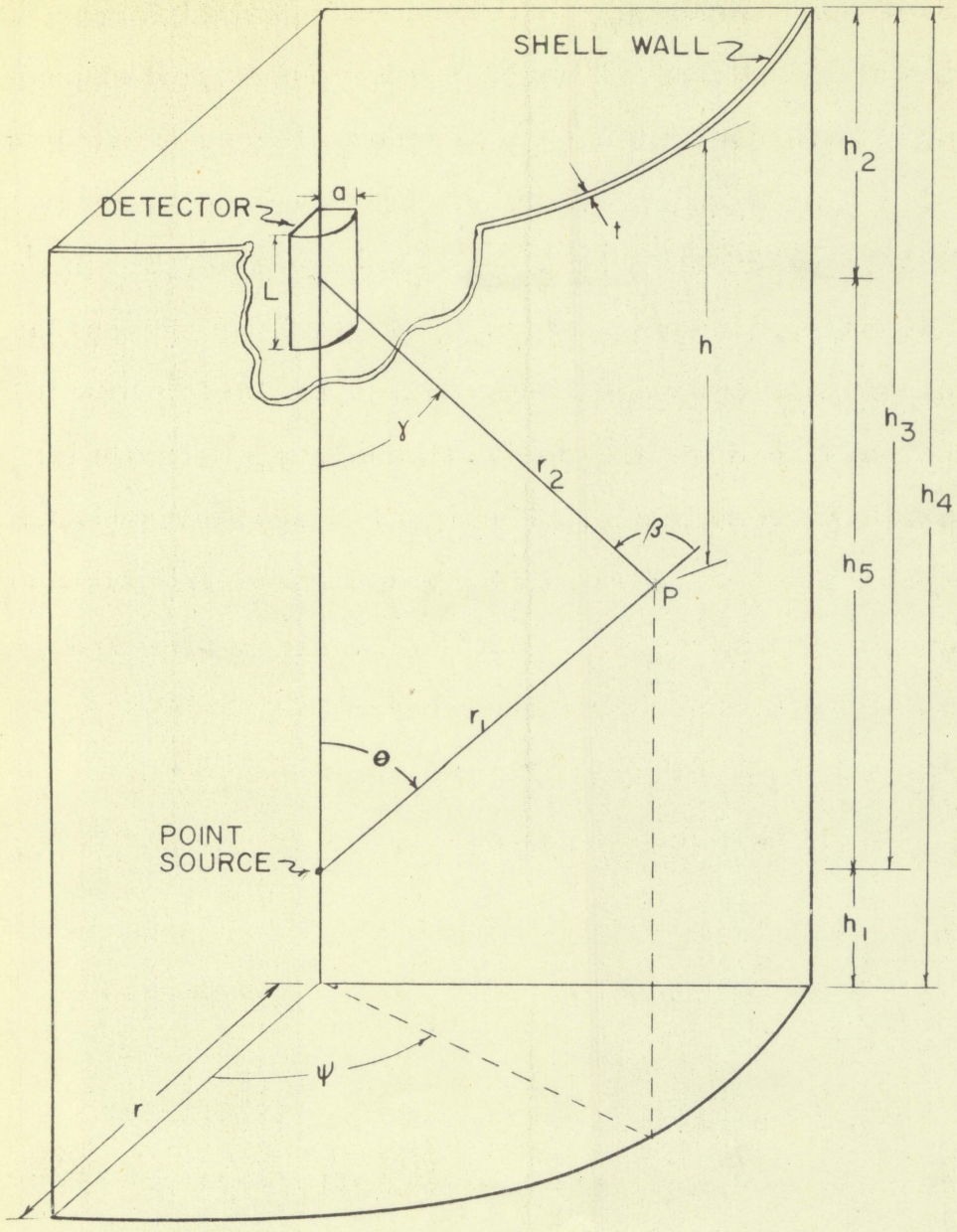

Figure 1. Geometry of scattering

Symbol	Units	Definition
$\frac{d\sigma}{d\Omega}$	$\frac{cm^2}{\text{electron, steradian}}$	Klein-Nishina differential collision cross section. The probability of a photon being scattered through angle β into an element of solid angle $d\Omega$ centered around β, where n_e is unity.
n_e	$\frac{\text{electrons}}{cm^3}$	Electron density of the scattering material.
n_s	$\frac{\text{photons}}{\text{second}}$	Number of gamma rays per unit time scattered into the detector by the shell wall.
a_o	Mev	Initial photon energy.
a	Mev	Photon energy after a Compton scattering reaction.
α	unit less	$\frac{a}{a_o}$
t_1	cm	Pathlength in the shell wall of an incident photon.
t_2	cm	Pathlength in the shell wall of an emerging photon.

The gamma ray flux ϕ_p incident on a unit area at point P in the shell wall is equal to $S\left(\frac{1}{4\pi r_1^2}\right)\left(e^{-\mu_a r_1}\right)\left(e^{-\mu_w t_1}\right)$. Here S, the total number of photons per second emitted isotropically from the source, is first multiplied by the probability of a photon being emitted in the direction of a unit area at distance r_1. This term $\frac{1}{4\pi r_1^2}$ is expressed as the ratio of the unit area to the entire surface area of a sphere with radius r_1. The product is then multiplied in turn by

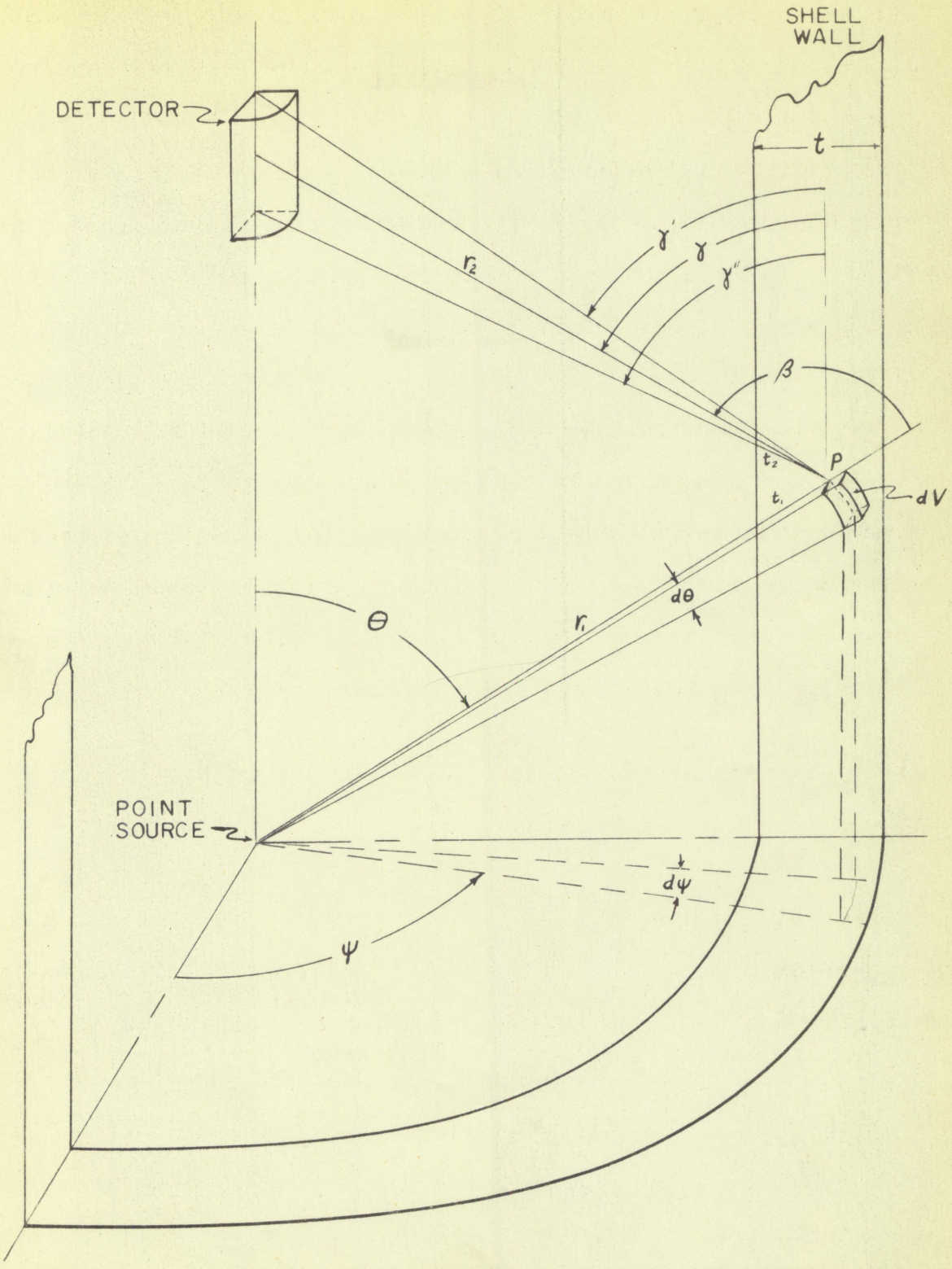

Figure 2. Differential scattering volume in shell wall

$\left(e^{-\mu_a r_1}\right)$, the probability of the photon passing through a distance $r_1 - t_1$ without being absorbed by the air, and $\left(e^{-\mu_w t_1}\right)$, the probability of passing through distance t_1 in the shell wall without being absorbed or scattered. The distance r_1 is so large compared to t_1 that the term r_1 may be used in place of $r_1 - t_1$ to represent the distance traveled in air by photon incident on P.

Now, a differential volume dV at P in a spherical coordinate system is chosen with dimensions $r_1 \sin\theta \, d\psi$, $r_1 d\theta$, and dr_1 as shown in Figure 2. The scattering which takes place in this differential volume is the product of the incident flux ϕ_p times the surface area $r_1 \sin\theta \, d\psi$, $r_1 d\theta$, times the probability of scattering in passing through a distance dr_1.

The Compton scattering process is not isotropic, but rather has a strong preference for forward, or small-angle scattering. The larger the angle scattered, the more energy is given up by the photon in the process, as indicated by the relationship,

$$\mathcal{R} = \frac{\alpha}{\alpha_o} = \left[1 + \frac{\alpha_o}{m_o c^2} (1 - \cos\beta) \right]^{-1}$$

where α_o is the initial photon energy, α is the final photon energy, β is the scattering angle and $m_o c^2$ is the rest energy of the recoiling electron. All energies are in Mev units.

The probability of a photon being scattered through a particular angle β was calculated by Klein and Nishina and is expressed as a cross section. Since the probability of scattering through an exact angle β is zero, it is necessary to specify a region, or solid angle Ω around the angle β, for which a finite probability can be expressed. This accounts for the differential cross section term $\frac{d\sigma}{d\Omega}$ which has the units of $\frac{cm^2}{electron}$ per steradian of solid angle.

The relationship between the differential collision cross section and β as found by Klein and Nishina is

$$\frac{d\sigma}{d\Omega} = \frac{r_e^2}{2} \frac{1}{[1 + \alpha_o(1 - \cos\beta)]^2} \left\{1 + \cos^2\beta + \frac{\alpha_o^2(1 - \cos\beta)^2}{1 + \alpha_o(1 - \cos\beta)}\right\}$$

where r_e is the classical electron radius.

Using the ratio of initial to final photon energies λ, the simplification is obtained,

$$\frac{d\sigma}{d\Omega} = \frac{r_e^2}{2} (\lambda - \lambda^2 \sin^2\beta + \lambda^3) \quad .$$

It is seen that the total probability of scattering in passing through the distance dr_1 is not sufficiently meaningful and, therefore, the probability of scattering into a particular solid angle is sought. Thus, in a volume element at P the number of photons scattered through an angle β per unit time in the direction of the detector may be expressed as

$$dn_s = \phi_P \frac{d\sigma}{d\Omega} \Omega_D \, n_e \, dV$$

where dV is the differential volume $(r_1 d\theta)$ $(r_1 \sin \theta \, d\psi)$ (dr_1), the term n_e is the number of electrons per unit volume of the scattering material, and Ω_D is the solid angle at P subtended by the detector.

The number of photons that arrive at the detector per unit time is equal to the number scattered in its direction multiplied by the respective probabilities, $e^{-\mu_w t_2}$, of passing through distance t_2 in the wall, and $e^{-\mu_a r_2}$, of passing through distance r_2 in the air without being absorbed or scattered.

The final expression for the number of photons, single-scattered into the detector by a unit volume dV is

$$dn_s = \phi_P \frac{d\sigma}{d\Omega} \Omega_D \, n_e \left(e^{-\mu_w t_2}\right) \left(e^{-\mu_a r_2}\right) dV$$

or, by expanding,

$$dn_s = \frac{S}{4\pi r_1^2} \left(e^{-\mu_a r_1}\right) \left(e^{-\mu_w t_1}\right) \frac{d\sigma}{d\Omega} \sin\theta$$

$$\Omega_D \, n_e \left(e^{-\mu_w t_2}\right) \left(e^{-\mu_a r_2}\right) r_1 \, d\theta \, r_1 \, d\psi \, dr_1$$

To solve for the total activity scattered from the entire cylinder, the differential volume is integrated between the geometrical limits for θ, ψ and r_1 as follows:

$$n_s = \int_{r_1} \int_{\psi} \int_{\theta} \frac{S}{4\pi} \; e^{-\mu_a (r_1 + r_2)} \; e^{-\mu_w (t_1 + t_2)}$$

$$\sin\theta \left(\frac{d\sigma}{d\Omega}\right) \Omega_D \, n_e \, d\theta \, d\psi \, dr_1$$

This resultant equation is considered generally applicable to the problem of single-scattered gamma rays within thin-walled cylindrical shells.

2. Simplifications and assumptions

For a particular application the expression obtained in the previous section is rather unwieldy, and any simplification which can be made for certain limited ranges of

scattering geometries will facilitate the evaluation of the integral.

If the scattering material is homogeneous, the electron density n_e is a constant. If the source is fairly constant or if its half-life is long with respect to the period under study, as is that of Cobalt-60, S may be considered a constant. Then this term and the other constant terms may be withdrawn from the integrand to obtain:

$$n_s = \frac{S\, n_e}{4\pi} \int_{r_1} \int_{\psi} \int_{\theta} e^{-\mu_a (r_1 + r_2)} \; e^{-\mu_w (t_1 + t_2)}$$

$$\sin\theta \left(\frac{d\sigma}{d\Omega}\right) \Omega_D \, d\theta \, d\psi \, dr_1$$

Mentioned briefly here are the treatments given to the several variable terms by the previous investigator. Following this is a discussion of the analysis of these terms by the present investigator with particular emphasis on the problems involved in their simplification.

The variable terms include: (1) Air Absorption. The non-absorption probability in air, $e^{-\mu_a (r_1 + r_2)}$, was investigated by Ney and found to be no less than 0.9935 for the maximum distances involved. This calculation is confirmed in the present study and the air absorption can be

considered negligible. (2) Wall Absorption. The matter of absorption in the shell wall was not treated at all. This term was not mentioned as a factor in the Ney study. (3) Differential Cross Section. Although the differential scattering cross section $\frac{d\sigma}{d\Omega}$ is a variable, the variation is quite small for large scattering angles β. Ney found this term to be fairly constant for scattering angles greater than 70°, and since few scattering angles smaller than this occurred in his study, he treated $\frac{d\sigma}{d\Omega}$ as a constant for the entire range concerned and withdrew it from the integrand. (4) Solid Angle. The solid angle subtended by the cylindrical detector Ω_D presented a particularly troublesome problem. An attempt was made to find this by a double integration over the area projected by the detector tube on the surface of a sphere passing through the center of the tube. Because the limits of integration were very hard to establish properly, the plane angle subtended by the diameter of the tube was considered constant and the vertical plane angle was integrated graphically for all locations of P in the shell wall. The result was an average value for Ω which was treated as a constant and withdrawn from the integrand.

The net equation of the previous study was

$$n_s = \frac{S\bar{\Omega}\, n_e}{4\pi} \frac{d\sigma}{d\Omega} \int_{r_1} \int_{\psi} \int_{\theta} d\theta\, d\psi\, dr_1$$

The variable dr_1 was integrated between the limits $\frac{r}{\sin\theta}$ and $\frac{r+t}{\sin\theta}$; then $d\psi$ was integrated between the constant limits $\psi = 0$ and $\psi = 2\pi$ giving an expression as a function of only one variable, θ.

$$n_s = \frac{S\,\bar{\Omega}\,n_e\,t}{2}\;\frac{d\sigma}{d\Omega}\int_{\theta}\frac{d\theta}{\sin\theta}$$

With the limits of θ established by the endpoints of the cylindrical shell, $\theta_1 = \tan^{-1}\frac{r}{h_3}$ and $\theta_2 = \tan^{-1}\frac{r}{h_1}$, this expression is easily solved by direct integration for each scattering geometry.

The present study is concerned with the problems in justifying the above simplifications and some other assumptions not justified in the previous study.

a. Wall absorption. A photon incident on the wall in the direction of P may be absorbed or scattered before reaching P; or, after being scattered at P toward the detector, it may be absorbed ~~or~~ before it passes out of the wall material. A limit analysis is made here to determine the significance of the wall absorption. The absorption probability is found for the maximum and minimum extremes encountered in the particular shells available for experimental study. The pathlength t_1 of the incident photon in the shell wall can have any value from zero to $\frac{t}{\sin\theta}$, Likewise, the wall path

length t_2 of the emerging photon scattered at P can have values from zero to $\frac{t}{\sin \gamma}$. For shells of finite length the maximum possible value of $t_1 + t_2$ occurs when the source and detector are nearly coincident at one extreme end of the shell and the scattering point P is in the opposite end in the outermost fiber of the wall. In this case θ and γ would be virtually equal and the total pathlength in the shell wall would be $\frac{2t}{\sin \theta}$ or

$$\frac{2t \sqrt{r^2 + h_4^2}}{r}.$$

The maximum possible pathlength is found for the most extreme shell available in this investigation. For the thickest shell with the smallest radius and greatest length, ($t = 0.250"$, $r = 3.0"$, $h_4 = 16"$), the maximum possible pathlength is found to be 6.89 cm. The probability of non-absorption in aluminum for a 1.25-Mev photon ($\mu_t = 0.150\ cm^{-1}$) passing this distance is $e^{-(0.150)\ (6.39)} = 0.356$.

Moreover, even in the case of the least severe geometry where the photon enters the material perpendicular to the surface and, after being scattered, emerges again perpendicular to it, the absorption probability becomes large as P approaches the outermost fiber of the shell wall. Here, $t_1 + t_2$ approaches 2t and the probability of non-absorption for the thickest shell (0.635 cm) is $e^{-(0.150)\ (2)\ (0.635)} = 0.826$. It must be concluded that non-absorption

probabilities on the order of 0.36 and 0.83 are too far from unity to be ignored. Therefore, the wall absorption term must be included in the theoretical scattering expression.

b. Second-scattered activity. The basic expression was developed under the presumption that all the shell-scattered photons arriving at the detector are singly scattered. However, it is intuitively obvious that the total scattered activity is the sum of an infinite series of terms representing the contributions from first scatters, second scatters, third scatters, etc. Now, if it can be shown that the contribution from second scatters is quite small with respect to the activity from first scatters alone, the third term can be shown to have the same relationship to the second term and, consequently, all terms except the one representing first scatters may be neglected.

Since the probability of a first scatter is very small, it seems reasonable to expect the probability of a second scatter to be correspondingly small with respect to the first and, hence, negligible with respect to the first scatter contribution. A limit analysis calculation was made to verify this expectation. It consisted essentially of first selecting a volume element at P in the shell wall. Then the activity scattered into the detector by this element was compared with that activity scattered first from P to other points on the shell and then scattered again into the

detector. To evaluate the second scatter a horizontal band of width Δh around the shell was selected at a value of h where the scattering contribution was near maximum. (The location of this region of maximum scattering contribution is discussed in Section V.) The volume element P was selected within this horizontal band.

The hypothesis of the limits analysis was as follows: If no other horizontal band contributes more than this "maximum" band, then the total activity, first-scattered in a unit volume at P and second-scattered by all other points in the shell into the detector will not exceed the total activity found by assuming all bands to be as important as this "maximum" band. Then, if the sum of the second-scattered activities from all such bands in the shell wall is quite small compared to the first-scattered activity, the second-scatter can be considered negligible in this limiting case and, consequently, in all cases.

Two postulates were helpful in finding the activity scattered by P into the horizontal band. First, the angle of a first-scatters from point P to any point in the narrow horizontal band is always equal to, or greater than 90°. Second, for scattering angles equal to, or greater than 90°, the differential scattering cross section, $\frac{d\sigma}{d\Omega}$, remains essentially constant for photons of 1.25 Mev. (See Figure 3) Therefore, a first-scatter from P in any horizontal direction toward the shell is equally probable.

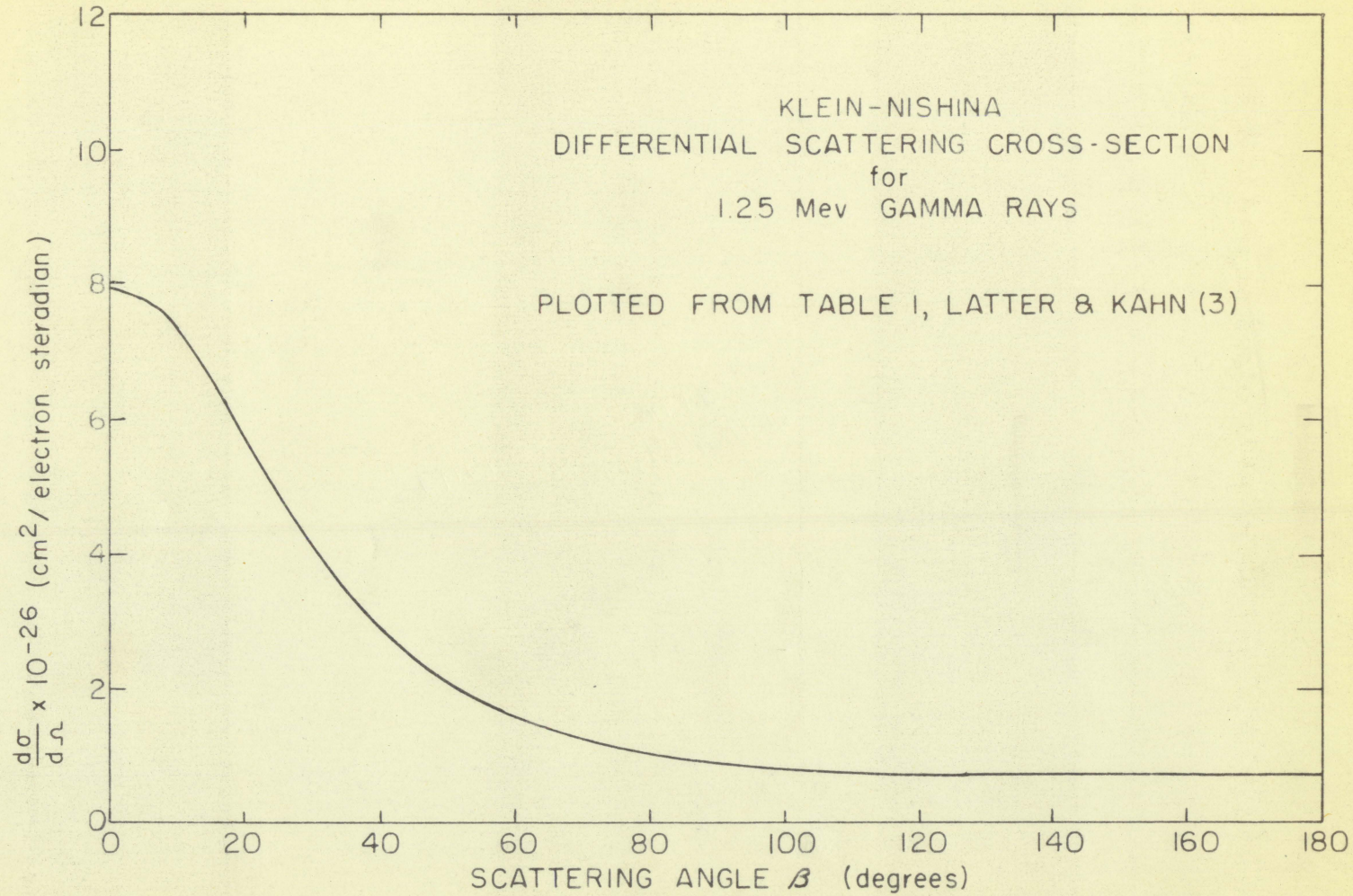

Figure 3. Variation in cross section with scattering angle

The horizontal plane angle (180°) subtended by the cylinder at point P in the wall was divided into six equal angles which intercepted six arcs on the horizontal band. For each of these arcs a representative point, P', was selected. Then the flux at P' from first-scatter in the volume element at P was calculated from the relationship:

$$\phi_{P'} = \phi_P \left(\frac{d\sigma}{d\Omega}\right)_P V_P n_e \Omega_{P'},$$

where V_P is the volume of the element at P, and $\Omega_{P'}$ is the solid angle subtended at P by a unit normal area at P'.

The flux $\phi_{P'}$ was considered to be a fair average value for all points in the arc represented by point P'. The flux at the detector ϕ_D, resulting from second-scatter in this arc can be expressed as:

$$\phi_{D'} = \phi_{P'} \left(\frac{d\sigma}{d\Omega}\right)_{P'} n_e \Omega_{D'} V_{P'},$$

where $V_{P'}$ is the volume of the arc of the horizontal band represented by P', and $\Omega_{D'}$ is the solid angle subtended by a unit normal area at the detector.

The total activity second-scattered from a unit volume at P into the detector by the entire horizontal band is the sum of the contributions from its several arcs. This activity is multiplied by the number of bands of width Δh

in the total shell length h_4 to give the total second-scatter contribution at the detector for photons first-scattered at P.

The calculation by this method for the most severe shell available (t = 0.250", r = 3.0", h_4 = 16") yielded for the second generation flux at the detector a value of $3.02 \times 10^{-7}\ \phi_p$, whereas the first generation flux was found to be $1.58 \times 10^{-5}\ \phi_p$.

It is seen that the second-scattered contribution is less than 2 per cent of the first-scattered contribution in the limiting case where all regions were considered to be as important as the maximum. Therefore, it can be concluded that the second-scattered activity, and, consequently, all activity from higher order scatter is very small compared with the first-scattered activity, and, hence, can be neglected.

c. Differential cross section. In the previous study the assumption was made that the scattering of photons in the shell wall was isotropic. This assumption was based on the Klein-Nishina differential collision cross sections for Cobalt-60 gamma rays, the values for which cross sections were evidently obtained from a graph in the literature of Plesset and Cohen (2). The previous study proposed that an average value of differential collision cross section $\frac{d\sigma}{d\Omega}$ for scattering angles greater than 70° could be employed as a constant in the development of the theoretical expression.

The reasons were that $\frac{d\sigma}{d\Omega}$ shows little variation for scattering angles greater than 70°, and few scattering angles smaller than this occurred in his study.

Neither of the two qualifying conditions is entirely satisfied. According to Latter and Kahn (3) who have tabulated precisely the values of $\frac{d\sigma}{d\Omega}$ for a wide range of gamma energies, the differential cross section varies between 0.697×10^{-26} $\frac{cm^2}{electron,\ steradian}$ for $\beta = 180°$, and 1.233×10^{-26} for $\beta = 70°$. Furthermore, scattering angles as small as 41° occur in the range of geometries studied, and for the shells of 3" radius the proportion of these small scattering angles becomes quite large. Two curves are included to show how the differential scattering cross section actually varies with the values of β encountered in the two extreme geometries investigated. Figure 4 is for the shell of smallest radius, 3", and Figure 5 is for the greatest radius, 8". It should be noted that the source-to-detector distance in both cases is the maximum possible within the end limits of the 16" shell length. For any distance h_5 less than 16" the scattering angles would be greater and the corresponding values of $\frac{d\sigma}{d\Omega}$ would be smaller. It is seen that Ney's use of the average value of 0.78×10^{-26} cm^2 per electron per steradian for $\frac{d\sigma}{d\Omega}$ is a satisfactory simplification for shells of large radii, but introduces a rather large source of error when applied to shells of smaller radii.

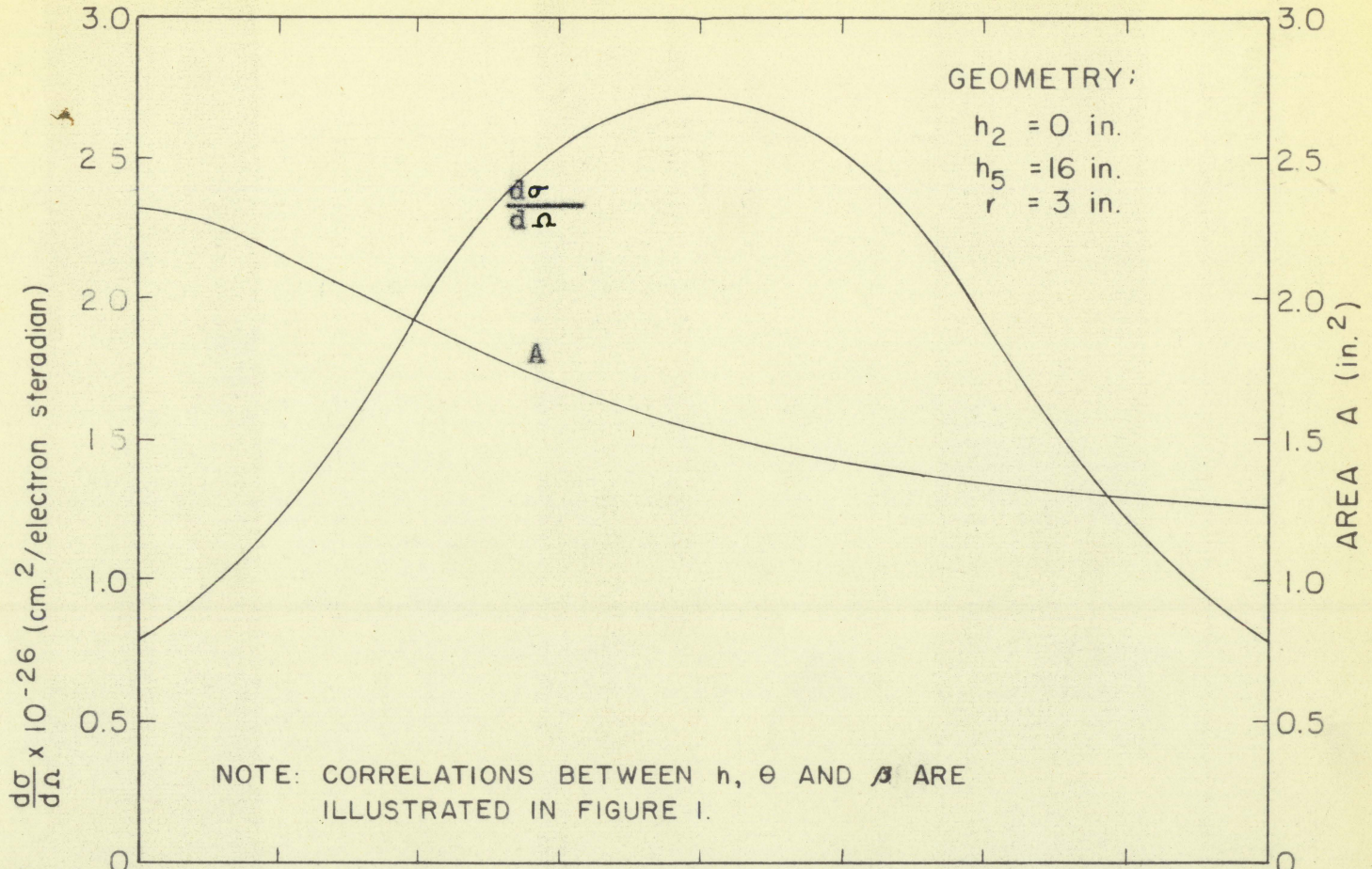

h (in.)	0	2	4	6	8	10	12	14	16
θ (degrees)	10.5	12	14	16.5	20.5	26.5	36.5	56	90
β (degrees)	101	69	51	43	41	43	51	69	101

Figure 4. Variation in $\frac{d\sigma}{d\Omega}$ and A with distance h in shell with smallest radius

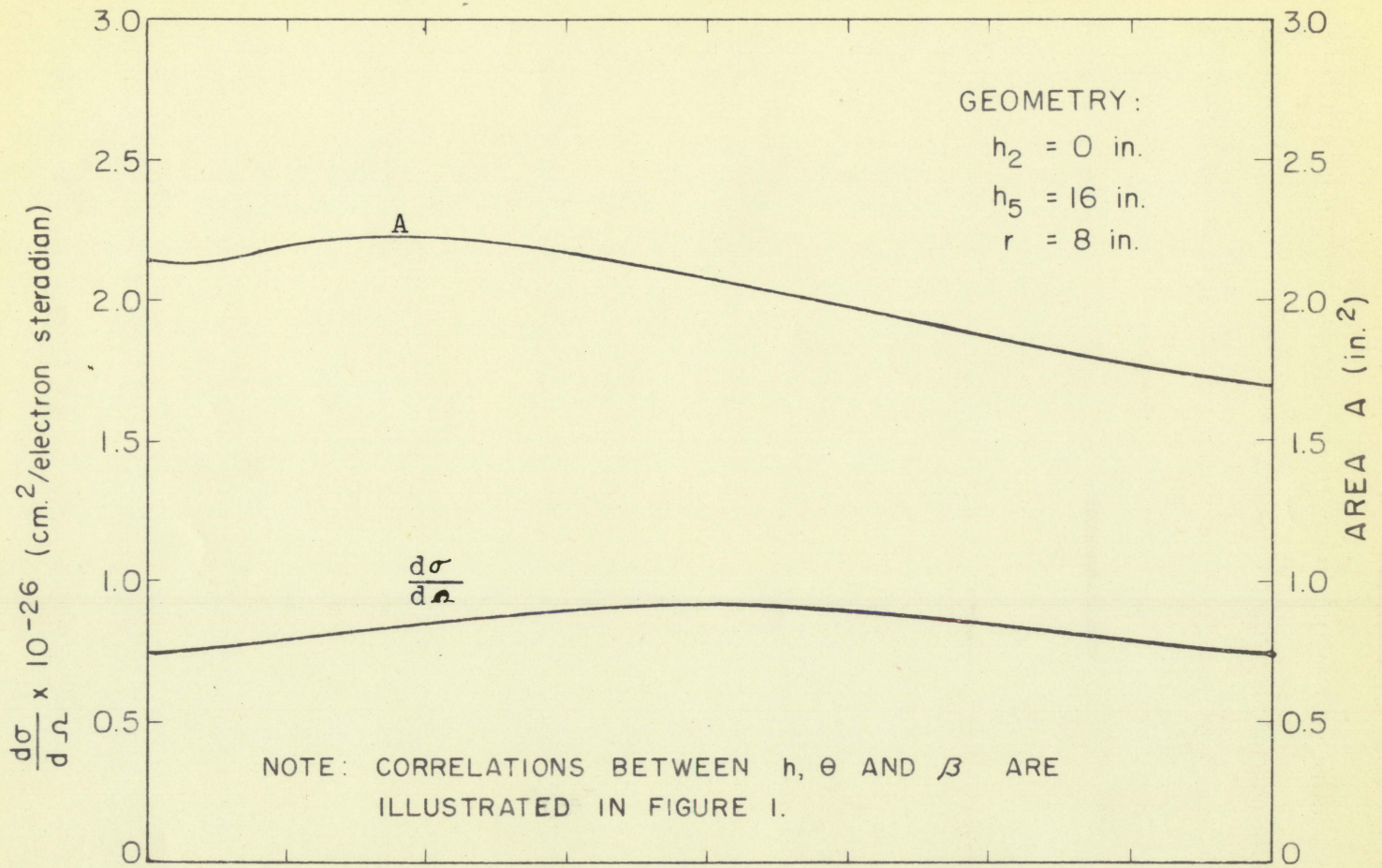

h (in.)	0	2	4	6	8	10	12	14	16
θ (degrees)	26.5	30	34	39	45	53.5	63.5	76	90
β (degrees)	116.5	106	97.5	92	90	92	97.5	106	116.5

Figure 5. Variation in $\frac{d\sigma}{d\Omega}$ and A with distance h in shell with largest radius

The conclusion of this analysis is that the treatment of $\frac{d\sigma}{d\Omega}$ as a constant is justified in a limited range of geometries where the shell radii are large and the source-to-detector distances are small. However, a more exact solution of the general problem requires that the differential scattering cross section be treated as a variable quantity.

d. Solid angle. The solid angle subtended by the detector is not easily determined because of the cylindrical shape of the G-M tube. Ney's approach to this difficulty consisted of finding the solid angle subtended by the area projected by the detector onto a spherical surface which passed through the center of the top of the counting tube. The surface was generated by swinging an arc of radius r_2 centered at the volume element P.

The solid angle Ω could be found from the double integration

$$\Omega = \int_{\delta_1}^{\delta_2} \int_{\gamma_1}^{\gamma_2} \sin\gamma \, d\gamma \, d\delta$$

where γ and δ represent the vertical and horizontal plane angles at P, respectively, and the subscripts 1 and 2 signify the limits of these angles subtended by the detector.

Since the limits on γ and δ are interdependent in a complicated manner due to the cylindrical shaped counter, Ney simplified the expression as:

$$\Omega = 2 \tan^{-1} \frac{a}{r} \int_{\gamma_1}^{\gamma_2} \sin\gamma \, d\gamma$$

This simplification assumes that the horizontal plane angle subtended by the detector remains constant for all scattering points. This assumption is not valid since $2 \tan^{-1} \frac{a}{r}$ is the horizontal plane angle subtended by the detector at only one value of h, that is, where the scattering point P is directly opposite the detector and r_2 is equal to r. For all other scattering points, r_2 is greater than r and the Ney expression will result in values for Ω that are too large.

When Ney's final expression for Ω was substituted into the complete scattering equation the result was the extremely complicated integral

$$n_s = \frac{3 n_e t}{2} \frac{d\sigma}{d\Omega} \int_{\theta_1}^{\theta_2} \left[2\tan^{-1} \frac{a}{r} \int_{\gamma_1}^{\gamma_2} \sin\gamma \, d\gamma \right] \frac{d\theta}{\sin\theta}$$

where, although γ and θ have a one-to-one correspondence, the resultant function of θ cannot be integrated analytically. To overcome this complication, Ney used an average value for Ω which was obtained by graphical integration between the limits imposed by the geometries of the available scattering shells. The solid angle was determined for each of sixteen values of h and the arithmetic mean of these sixteen determinations was used for the average solid angle $\bar{\Omega}$. Then $\bar{\Omega}$ was removed from the integrand to leave the final scattering expression:

$$n_s = \frac{S\, n_e\, t\, \bar{\Omega}}{2} \frac{d\sigma}{d\Omega} \int \frac{d\theta}{\sin \theta} .$$

The method of using an arithmetic mean for $\bar{\Omega}$ assumes that all scattering points are equally significant to the overall scattered activity. This assumption is invalid as shown in Figure 6 which illustrates the relative scattering importance of the various regions of the shell.

Thus, it is seen that the previous investigator's approach to the problem of the solid angle subtended by the detector was basically sound, but two of the simplifying assumptions made were invalid. The present study is concerned with means of achieving a useful expression for the solid angle term without depending on these two assumptions. The expression used here to find the solid angle is

$$\Omega = \frac{A}{r_2^2}$$

where A is the area the detector projects on a plane perpendicular to the radius r_2.

If it can be shown that A is a constant or nearly constant, then the integral $\int \Omega \, d\theta$ can be expressed as $A \int \frac{d\theta}{r_2^2}$ which can be integrated analytically. The area A may be represented by $A = A_s \sin\gamma + A_e \cos\gamma$ where A_s is the projected rectangular area of the side or wall of the detector on a plane through its longitudinal axis, A_e is the area of the circular end of the detector, and γ is the angle formed at the center of the detector by the longitudinal axis and the radius vector r_2.

The perpendicular areas A_e and A_s are assumed to be located at the midpoint of the detector. A small error introduced by this assumption occurs when the scattering point P is located directly opposite the detector. In this region the $A_e \cos\gamma$ term decreases and becomes zero. Actually, the contribution to A from the ends of the counting tubes never completely disappears. Therefore, a more exact expression can be written which does not assume that A_e is located at the midpoint of the detector, but instead represents the actual situation where half of A_e appears at the bottom of the counter and half at the top. This expression is

$$A' = A_s \sin \gamma + \frac{A_e}{2} \cos \gamma' + \frac{A_e}{2} \cos \gamma''$$

where the area is designated A', and γ' and γ'' are the angles formed at P by the vertical wall and the radius vectors to the center of the counter bottom and counter top respectively.

The expressions for A and A' are plotted as functions of h to illustrate the effect of using the corrected expression, and also to show the extent of the variation in this area term with location of scattering point P in the shells of smallest and largest radii 3 inches and 8 inches, respectively. (See Figures 4 and 5).

Two conclusions can be drawn from the curves: The values of A and A' are so nearly alike there is little advantage in using the more exact expression; and although the variation in A with h is significant for the shells of small radii, the projected area term becomes nearly constant for shells of large radii. The curves are plotted for the extreme case where the center of the detector is at h = 0. A detector location at any other value of h would yield a smaller variation in A than the cases illustrated. It is seen that certain simplifications are essential in order to obtain an equation that can be solved. Where the range of application is limited, it is possible to treat the terms $e^{-\mu_w(t_1 + t_2)}$, $\frac{d\sigma}{d\Omega}$ and A as constants and use the expression

$$n_s = \frac{S\ t\ n_e}{2} \overline{\frac{d\sigma}{d\Omega}} \overline{A\ e^{-\mu_w(t_1 + t_2)}} \int \frac{d\theta}{r_2^2}$$

which can be integrated directly. On the other hand, if the limits of the application are broad and the terms $\frac{d\sigma}{d\Omega}$, A and $e^{-\mu_w(t_1 + t_2)}$ vary considerably over the given range, then they must be retained in the expression as variables. In such cases the equation cannot be integrated directly and a graphical solution must be employed. In the present study an analytical solution for the integral $\int \frac{d\theta}{r_2^2}$ and a graphical solution was obtained for the expression

$$n_s = \frac{S\ n_e\ t}{2} \sum \frac{d\sigma}{d\Omega} \frac{A}{r_2^2} e^{-\mu_w(t_1 + t_2)} \Delta\theta \quad .$$

Only the latter solution was found to be sufficiently useful for the present study.

B. Solution of Equation

1. Evaluation of terms.

In order to solve the theoretical expression for particular cases, it is necessary to evaluate the terms involved. The terms here are evaluated for the particular materials and geometries encountered in the experimental

portion of this study. Briefly, the materials consisted of 24ST aluminum alloy shells, some of which were Alclad, an end-window G-M tube, and a small Cobalt-60 source. These are described more fully in the experimental section.

a. Source term. The source term S was evaluated from the relationship $n_D = S \frac{\Omega_E}{\Omega}$ where n_D is the number of photons radiated directly into the end of the detector per unit time, Ω_E is the solid angle subtended by the end of the detector, and Ω is the total solid angle. If d is the distance from the source to the end of the detector, and a is the radius of the detector, then

$$n_D = S \frac{\pi a^2}{4\pi d^2}$$

The counting rate for direct radiation is

$$R_D = \epsilon n_D = \epsilon S \frac{a^2}{4d^2}$$

where ϵ is the counting efficiency of the detector.

There was no particular advantage in determining the exact strength of the gamma source, even if it could have been done. Since the counting efficiency of the G-M detector was not known but is generally on the order of one per cent, the source term was considered to be proportional to the counting rate and no attempt was made to determine the absolute source strength. Therefore, the product ϵS

is represented as S' and has the units of counts per minute. The term ϵ' absorbs the difference in units.

The detector radius a and the counting rate R_D could be measured directly. However, the distance d was difficult to measure because the exact location of the effective end of the detector was unknown. In other words, the mica window could not be considered as the effective end of the tube since most of the interactions occur in the tube cover. Therefore, the effective end of the tube was determined through an indirect method. This method consisted of measuring the direct counting rate for two widely separated values of the distance, h_5.

From the relationship $R_D = S'\frac{a^2}{4d^2}$, where $d = h_5 - x$, the unknown distance x from the detector midpoint to the effective end wall was determined. The distance x was presumed to be constant. Therefore, its value could be found by the simultaneous solution of

$$R_{D_1} = S'\frac{a^2}{4(h_{5_1} - x)^2},$$

and

$$R_{D_2} = S'\frac{a^2}{4(h_{5_2} - x)^2}.$$

The distance x was found to be 0.20 inch which in turn was used in the same equation to find the value, 4.012×10^6 counts per minute for S'.

b. Electron density. The term n_e was determined from the composition of the aluminum used in the experiment. The 24ST aluminum alloy has a nominal composition (4) of 93.4 per cent aluminum, 4.5 per cent copper, 0.6 per cent manganese, and 1.5 per cent magnesium. Although small amounts of some impurities may be present, their contributions to the electron density of the alloy are negligible. A value of 7.99×10^{23} electrons per cm^3 was found, using the relationship

$$n_e = N_A \rho \left[\frac{f_{Al} Z_{Al}}{A_{Al}} + \frac{f_{Cu} Z_{Cu}}{A_{Cu}} + \frac{f_{Mn} Z_{Mn}}{A_{Mn}} + \frac{f_{Mg} Z_{Mg}}{A_{Mg}} \right]$$

Here, N_A in Avogadro's number, ρ is the density (2.77 gm/cm^3), f is the weight fraction, Z is the atomic number and A is the atomic weight.

The electron density of the cladding, which is essentially pure aluminum, was found to be 7.88×10^{23} electrons per cm^3. Since the cladding composes 5 per cent of the total weight of sheets with thickness of 0.064" or greater, and 10 per cent for sheets less than 0.064" thick, a value of electron density of 7.98 electrons per cm^3 may be used without significant error for all shells concerned in this study.

2. Analytical method.

The theoretical equation was solved both analytically

and graphically. In order to obtain an expression that could be integrated analytically it was necessary to find average values for several variables and by treating them as constants, remove them from the integral. Such simplification has certain inherent shortcomings as pointed out in the section on Simplifications and assumptions. However, if the terms remain fairly constant over the given range, or if proper, weighted-average values can be found for the variables, then the simplified analytical solution may be used. The present section describes the analytical solution of the integral $\int \frac{d\theta}{r_2^2}$

Let $y = \int \frac{d\theta}{r_2^2}$

From Figure 1 it is seen that $r_2 = \frac{r}{\sin \gamma}$ and by the law of cosines

$$r_2^2 = h_5^2 + r_1^2 + 2h_5 r_1 \cos \theta$$

However since $r_1 = \frac{r}{\sin \theta}$, then $r_2^2 = r^2 + (h_5 - r \cot \theta)^2$.

Let $a = \frac{h_5}{r}$

$$y = \frac{1}{r^2} \int \frac{d\theta}{1 + (a - \cos \theta)^2}$$

Let $x = (a - \cot \theta)$ and $dx = \csc^2 \theta \, d\theta$.

Then by trigonometric substitution, $dx = \left[(a - x)^2 + 1\right] d\theta$.

Thus $$y = \frac{1}{r^2} \frac{dx}{\left[(a - x)^2 + 1\right] \left[1 + x^2\right]}$$

Now, by the method of partial fractions,

$$\frac{1}{\left[1 + x^2\right] \left[1 + (a - x)^2\right]} = \frac{Ax + B}{1 + x^2} + \frac{C + D(a - x)}{1 + (a - x)^2} .$$

and $$r^2 y = A \int \frac{x\,dx}{1 + x^2} + B \int \frac{dx}{1 + x^2}$$

$$+ C \int \frac{dx}{1 + (a - x)^2} + D \int \frac{(a - x)\,dx}{1 + (a - x)^2}$$

where A, B, C and D are undetermined coefficients.

Then $$1 \equiv \left[Ax + B\right] \left[1 + (a - x)^2\right]$$

$$+ C(1 + x^2) + D(a - x)(1 + x^2) .$$

Since the coefficients of like powers of x must be equal, four equations can be written to evaluate the four undetermined coefficients. The values found for these are,

$$A = D = \frac{2}{a(4 + a^2)} \qquad B = C = \frac{1}{(4 + a^2)}$$

Since the four integrals have the following solutions

$$\int \frac{x\,dx}{1 + x^2} = \frac{1}{2} \ln (x^2 + 1)$$

$$\int \frac{dx}{1 + x^2} = \tan^{-1} x$$

$$\int \frac{dx}{1 + (a - x^2)} = \tan^{-1} (x - a)$$

$$\int \frac{(a - x)\,dx}{1 + (a - x)^2} = -\frac{1}{2} \ln \left[1 + (a - x)^2\right]$$

the final solution can be simplified as

$$r^2 y = \frac{1}{a(4 + a^2)} \left[\ln \frac{x^2 + 1}{1 + (a - x)^2}\right] + \frac{1}{(4 + a^2)} \left[\tan^{-1} x + \tan^{-1} (x - a)\right] .$$

Replacing x with a - cot θ

$$r^2 y = \frac{1}{a(4 + a^2)} \left[\ln \frac{(a - \cot \theta)^2 + 1}{1 + \cot^2 \theta}\right] + \frac{1}{(4 + a^2)} \left[\tan^{-1} (a - \cot \theta) + \theta - \frac{\pi}{2}\right] .$$

Thus

$$y = \frac{1}{4r^2 + h_5^2} \left[\frac{r}{h_5} \ln \frac{\frac{h_5}{r} - \cot^2 + 1}{1 + \cot^2 \theta} \right]$$

$$+ \tan^{-1} \left[\frac{h_5}{r} - \cot \theta \right] + \theta - \frac{\pi}{2}$$

which is the desired solution to the integral

$$\int \frac{d\theta}{r_2^2}$$

Although an analytic solution is obtainable it is not sufficiently useful for wide application because it does not treat enough of the variable terms. The more straightforward graphical solution, on the other hand, proved to be more easily evaluated, and furthermore, it had the additional advantage of treating the solid angle, cross section, and wall absorption terms as variables.

3. Numerical method

The solution to the general expression

$$n_s = \frac{S\, n_e\, t}{2} \int_{\theta} \frac{d\sigma}{d\Omega} \frac{A}{r_2^2} e^{-\mu_w(t_1 + t_2)}\, d\theta$$

was approximated by expressing it as the sum

$$n_s = \frac{S\, n_e\, t}{2} \sum_{\theta_1}^{\theta_2} \frac{d\sigma}{d\Omega} \frac{A}{r_2^2} e^{-\mu_w(t_1 + t_2)}\, \Delta\theta \quad .$$

Specific values for each of the variable terms, $\frac{d\sigma}{d\Omega}$, A, $e^{-\mu_w(t_1 + t_2)}$ and $\frac{1}{r_2^2}$ were determined for each of several increments of angle θ between θ_1, corresponding to the top rim of the shell and θ_2 representing the bottom rim. The product of the variable terms was plotted as a function of θ and the area under the curve represented the desired solution of the summation.

The differential collision cross sections were taken from Figure 3. The values for this curve were interpolated from cross sections in Table 1 of Latter and Kahn (3). The areas A were determined from the relationship

$$A = A_s \sin\gamma + \frac{A_e}{2} (\cos\gamma' + \cos\gamma'') \quad .$$

Non-absorption probabilities were calculated from the total absorption coefficient of 1.25-Mev photons in aluminum and the relationship

$$\overline{t_1 + t_2} = \frac{t}{2r}(r_1 + r_2)$$

which is based on a scattering point located midway through the shell wall. The terms $\frac{1}{r_2^2}$ and $\frac{\sin^2\theta}{r}$ were calculated directly from the geometry of the scattering points.

Since a uniform increment of angle θ represented such a large portion of the shell wall at small values of θ, and conversely, such a small portion of the wall for values of θ near $\frac{\pi}{2}$, a poor distribution of points resulted. Therefore, the variable of summation was shifted from increments of angle θ to increments of shell length h in the following manner.

$$r_1 \, \Delta\theta = \sin\theta \, \Delta h \qquad \text{where } r_1 = \frac{r}{\sin\theta}$$

Thus $$\Delta\theta = \frac{\sin^2\theta}{r} \, \Delta h$$

yielding the final expression

$$n_s = \frac{S \, n_e \, t}{2} \sum_{h=0}^{h=16} \frac{d\sigma}{d\Omega} \frac{A}{r_2^2} \, e^{-\mu_w(t_1 + t_2)} \frac{\sin^2\theta}{r} \, \Delta h$$

Values for the product of the variable terms were determined for one-inch increments of h and plotted as a function of h. Figure 6 illustrates this plot for one of the investigated geometries, where the detector is located at h = 4 inches and the source is located at h = 12 inches. The area under the curve representing the sum, was then multiplied by the constant terms $\frac{S\, n_e}{2}$ and the shell thickness t, to yield the net scattered activity n_s. The tabulated data used in finding the solutions by the graphical summation method are included in the Appendix. The final solutions found by this method are plotted in Figure 8, Section V where they are compared with the corresponding values determined by experimental measurement.

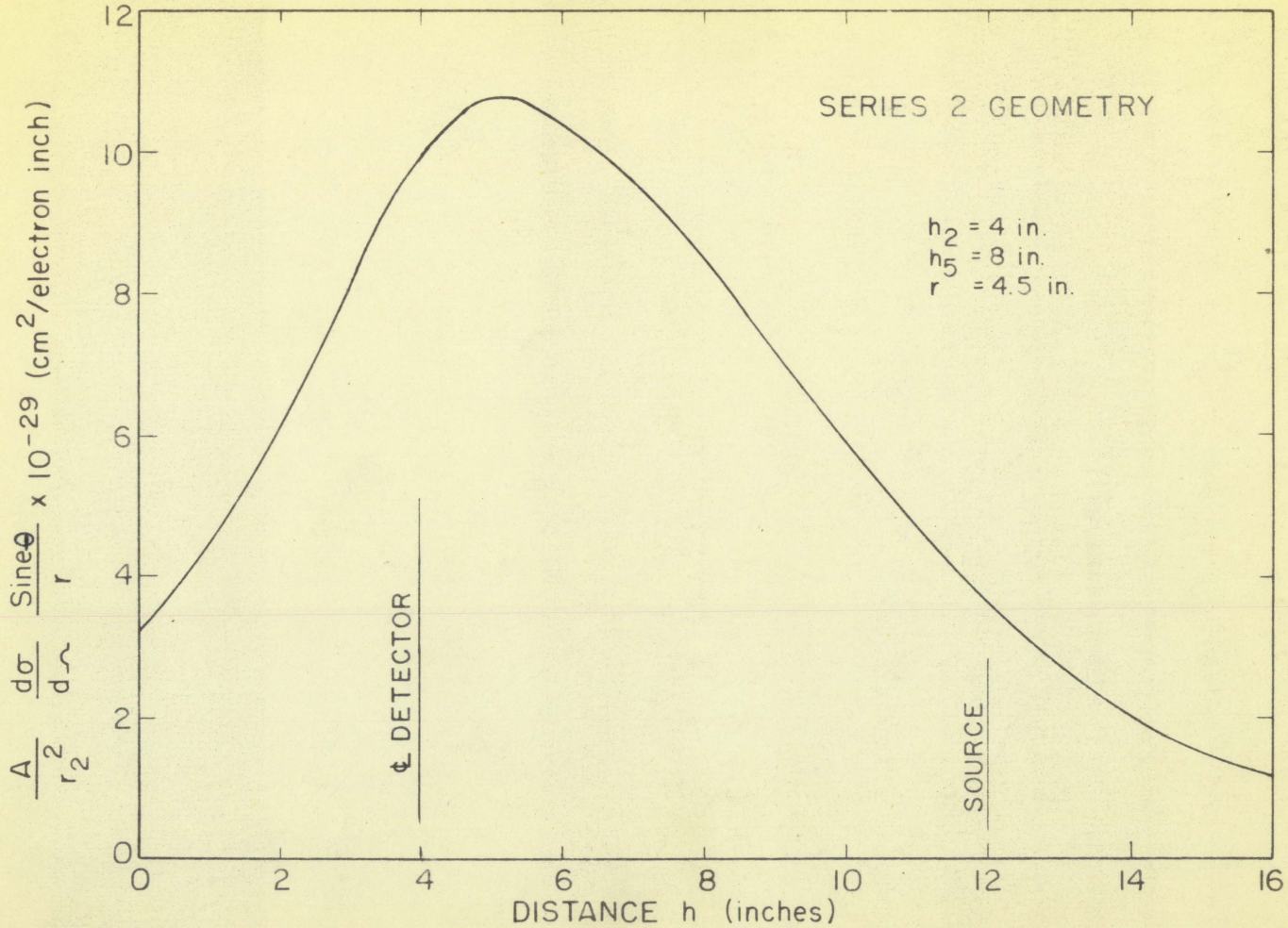

Figure 6. Relation between the contribution of a scattering point and its location in the shell wall

IV. EXPERIMENTAL PROGRAM

A. Difficulties of Previous Study

When K. C. Ney investigated experimentally the scattering of gamma rays in cylindrical shells, he encountered certain difficulties which rendered his experimental findings inconclusive. His procedure is briefly outlined here with some elaboration on the specific areas where some of the sources of difficulty may lie.

The equipment used by Ney consisted of the following major items:

(1) Deci-scaler, Radiation Instrument Laboratories, Model 200.

(2) Geiger counter, Tracerlab TGC-8, 1.5" diameter, 2.375" long.

(3) Gamma source, approximately 10 microcuries of Co^{60} wrapped in cellophane tape to form a small cylinder about 1" long and 1/4" in diameter.

(4) Seven cylindrical aluminum shells, 16" long, with particular parameters as listed below:

Thickness (in.)	Material	Radius (in.)
0.025	24ST	3.0
0.025	24ST	4.5
0.025	24ST	6.0
0.064	Alclad 24ST	6.0
0.064	Alclad 24ST	8.0
0.126	Alclad 24ST	4.5
0.126	Alclad 24ST	8.0

The experimental procedure may be summarized briefly as follows: The small source, treated here as a point source, was suspended directly beneath the detector at a distance of either 4" or 6". Around the detector was positioned one of the open-ended cylindrical shells such that its longitudinal axis was coincident with the longitudinal axis of the detector and of the source. The upper end of the detector was maintained at the same elevation as the upper end of the scattering shell. The whole assembly was located just above the floor, on which was placed a 1-1/2" thick layer of lead. (The literature does not specify whether the scattering shells actually rested on the lead, but it is presumed that they did.)

At a source-to-detector distance of 4", a five-minute counting measurement was made with each of the seven shells in position. With the same arrangement of the apparatus, another five-minute count was taken without any shell in place. Then the source-to-detector distance was set at 6" and another eight measurements were made, this time for a ten-minute duration each.

The net counting rate R_t was considered to be the sum of R_D, the activity radiated directly into the detector from the source; R_W, the activity scattered into the detector by the air and objects in the room; and R_S, the activity scattered into the detector by the cylindrical shell (in those measurements where the shell was employed). The

activity scattered into the detector by the air and room, R_W, was considered to be constant, independent of either the aluminum shells or small changes in the source-to-detector distance. The activity radiated directly into the detector from the source was considered to be dependent on the source-to-detector distance by the relationship $R_D = \frac{S}{2}(1 - \cos \beta_d)$, where S is the source term and β_d is the plane angle at the source subtended by the radius of the detector tube end.

The air-room scattering rate R_W was determined from the ratio of two direct radiation rates, $(R_D)_4$ and $(R_D)_6$, corresponding to the 4" and 6" source-to-detector distances respectively.

$$\frac{(R_D)_4 = \frac{S'}{2}(1 - \cos \beta_4)}{(R_D)_6 = \frac{S'}{2}(1 - \cos \beta_6)}$$

The value found for this ratio was then substituted into the equation,

$$\frac{(R_D)_4}{(R_D)_6} = \frac{(R_t)_4 - R_W}{(R_t)_6 - R_W} \quad .$$

The relationship $R_D = R_t - R_W$ is applicable to the counting rates when no shells are employed, i.e. when $R_S = 0$. Using experimental values of 4752 ± 31 and 2587 ± 17 respectively for $(R_t)_4$ and $(R_t)_6$ in this equation, Ney obtained a value of 782 ± 41 counts per minute for R_W. The counting rates for all measurements employing shells were then corrected by this amount to obtain the net shell-scatter rates R_S from the relationship

$$R_S = R_t - R_W - R_D \quad .$$

The final result of each measurement was expressed as the ratio of the total counting rate to the direct counting rate,

$$\frac{R_S + R_D}{R_D}$$

This ratio was represented by the symbol R_{T_γ}. The technique of expressing the results as ratios permitted the cancellation of constant terms common to counting rates from both scattered and direct radiation.

The following table, extracted from Ney's thesis, gives the results of his gamma ray scattering measurements along with the results obtained from his theoretical analysis. In the table, h_5 is the source-to-detector distance, and R_{W_γ} is the air and room scattering rate. The smaller standard deviations in the net counting rates for the last eight

Table 1

Gamma ray counting rates corrected for air and room scattering and total gamma ray scattering ratios

Cylindrical shell dimensions r (in.)	t (in.)	h_5 (in.)	Net counting rate (R) (counts per minute)	$R - R_{W_\gamma}$ (counts per minute)	R_{T_γ} experimental	R_{T_γ} theoretical
none		4	4752 ± 31	3970 ± 51		
3	0.025	4	4823 ± 32	4041 ± 52	1.018 ± 0.019	1.010
4.5	0.025	4	4853 ± 32	4071 ± 52	1.025 ± 0.019	1.005
6	0.064	4	4798 ± 32	4016 ± 52	1.012 ± 0.018	1.007
4.5	0.126	4	4875 ± 32	4093 ± 52	1.031 ± 0.019	1.024
8	0.126	4	4851 ± 32	4069 ± 52	1.025 ± 0.019	1.007
none		6	2587 ± 17	1805 ± 44		
3	0.025	6	2685 ± 17	1903 ± 44	1.055 ± 0.036	1.023
4.5	0.025	6	2605 ± 17	1823 ± 44	1.010 ± 0.035	1.010
6	0.025	6	2610 ± 17	1828 ± 44	1.013 ± 0.035	1.006
6	0.064	6	2650 ± 17	1868 ± 44	1.035 ± 0.035	1.015
8	0.064	6	2597 ± 17	1815 ± 44	1.006 ± 0.035	1.008
4.5	0.126	6	2731 ± 17	1949 ± 44	1.080 ± 0.036	1.052
8	0.126	6	2643 ± 17	1861 ± 44	1.031 ± 0.035	1.016

measurements are largely a result of the longer, 10-minute counting periods as contrasted to the 5-minute periods used in the first six measurements.

Ney's results, expressed as ratios of the total counting rates to the direct radiation counting rates, gave values very close to unity. The statistical deviations in the results, however, were so large that the data were not conclusive. Ney attributed the cause of the large statistical deviations to the air and room scatter, which he felt must be considerably reduced in order to improve the statistics. Actually, it appears that the contribution from air and room scatter was not the major source of uncertainty, but instead, the error results from the attempt to find the difference between two large and nearly equal values. For example, the data for the first shell may be analyzed as follows:

Less	Total Counting Rate	(Measured)	4823 counts/min.
	Air-Room Scatter Rate	(Calculated)	- 782
			4041
Less	Direct Radiation Rate	(Calculated)	-3970
	Net Shell Scatter Counting Rate		71 counts/min.

It is apparent that the radiation, scattered by the air and the objects in the room, is somewhat less significant than the direct radiation contribution. In fact, a 1 per cent error in the calculated value of R_D would produce a 56 per cent error in the net shell scatter rate R_S.

Furthermore, the calculation of R_D called for evaluating the term $(1 - \cos \beta_d)$ for rather small values of β_d. This procedure, once again, introduced the large source of error that accompanies finding the difference between two nearly equal values.

In the present study an attempt was made to repeat the experimental work done by Ney and to make some refinements that would reduce the sources of error that he encountered. The specific areas in which improvement was sought include: (1) Reduction of the extremely large contribution from direct radiation to the total counting rate, (2) Reduction of the room scatter contribution, (3) Reduction of the uncertainties in the counting statistics, and (4) Expression of the findings in such a manner that their significance may be more readily apparent.

B. Equipment and Materials

The equipment and materials employed in the present study were essentially the same as those employed by K. C. Ney in his experimental work, with a few variations and additions. The equipment which was identical in both studies included the Deci-scaler, Model 200, manufactured by Radiation Instrument Laboratories, and the seven aluminum shells mentioned above which were prepared for Ney by the Iowa State College Instrument Shop.

In addition to the seven shells used previously, ten more shells, prepared by the Instrument Shop, were used in the present study. The sizes of these shells (indicated by asterisks in Table 2) were chosen in an effort to obtain experimental data to illustrate the effect of varying only one parameter at a time. The three parameters to be varied were length, radius, and wall thickness. Although the composition varied among the shells, the difference between the pure alloy and the Alclad shells has practically no effect on the gamma scattering as was shown in Section III, B, 1.

The detector used was a Nuclear-Chicago mica end-window Geiger-Mueller tube, type D-33. It was employed with the cover on the window and operated at 950 volts throughout the study. The location of the midpoint of the active volume was found by first determining the effective length of the detector. The detector volume was not exactly cylindrical but was somewhat bullet-shaped. To find this volume a discarded tube, a duplicate of the one used in this study, was filled with water from a graduated burette. The inside diameter was measured directly and the effective length of an equivalent cylinder was calculated from $V = \pi r^2 h$ and found to be 4.9 cm. The midpoint of the detector length was taken to be 2.45 cm from the window.

Table 2

Cylindrical shells employed in experimental program

Thickness (in.)	Material	Radius (in.)	Length (in.)
0.025	24ST	3.0	16
0.025	24ST	4.5	16
0.025	24ST	6.0	16
0.063*	Alclad 24ST	3.0	16
0.063*	Alclad 24ST	3.0	24
0.063*	Alclad 24ST	3.0	32
0.064*	Alclad 24ST	4.5	16
0.064	Alclad 24ST	6.0	16
0.064	Alclad 24ST	8.0	16
0.126*	Alclad 24ST	3.0	16
0.126	Alclad 24ST	4.5	16
0.126*	Alclad 24ST	6.0	16
0.126	Alclad 24ST	8.0	16
0.250*	24ST	3.0	16
0.250*	24ST	4.5	16
0.250*	24ST	6.0	16
0.250*	24ST	8.0	16

*Shells used exclusively in present investigation.

As a means of improving the counting statistics, a stronger gamma source was used. This source, approximately 100 microcuries of Co^{60}, was prepared by the Health Physics Group of the Ames Laboratory on January 23, 1956. Its strength, at the time of this study one year later, was approximately 88 microcuries, determined from its half-life of 5.3 years. Since the source strength diminishes only 1% in 28 days, the gamma source was considered to be constant for

the duration of the experimental measurements which required less than one month.

The source was in a small aluminum, disc-shaped container, 1/2 inch in diameter and 1/8 inch thick. The active material was located in the center of the disc and could be considered as a point source for the purposes of this study. On one face of the disc was a small lug with an eyelet for suspending the source by a string.

C. Procedure

The problem of radiation scattered into the detector by the walls and fixtures in the room was combated by isolating the experiment from these objects as much as possible. The shell, source and detector were positioned midway between the floor and the ceiling, and at least as far from any walls. The source was suspended from the ceiling by a length of braided linen cord, and directly below it was placed the detector, supported by a bare, wooden framework. (See Figure 7). The framework also supported the shells which were placed one at a time coaxially around the detector. This set-up required a minimum of rearranging each time the shells were changed. The source was simply raised out of the shell far enough to make the change and lowered back to the same level afterward. The frame support was marked with arcs of 3 inch, 4.5 inch, 6 inch and 8 inch

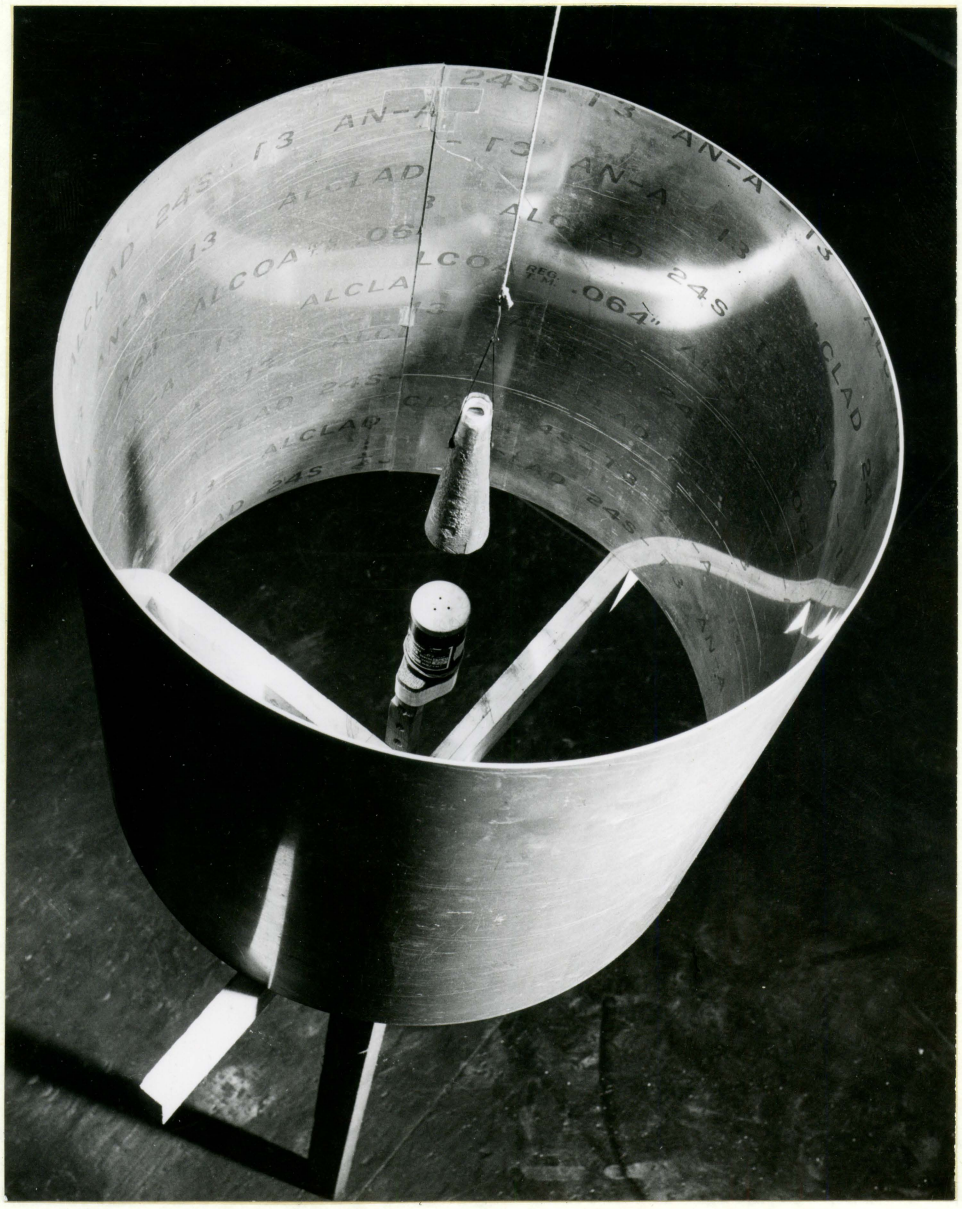

Figure 7. Experimental arrangement of shell, detector and shadow shield

radius circles to provide a means of easily reproducing the scattering geometry from one test to the next.

The major problem of the previous investigator was that of trying to determine accurately the small difference between the large total counting rate and the almost-as-large direct radiation counting rate. In order to eliminate this difficulty in the present study, a lead shadow shield was placed between the source and detector to absorb the direct radiation. The shield was a truncated cone about 4 inches long with a 1-3/8 inches diameter base and a 1/2 inch diameter top where the source was placed. This shape provided that the detector was completely in the umbra of the shield for all geometries investigated.

The experimental program consisted of five series of measurements, each series representing a different value of source-to-detector distance, h_5. Distances of 6 inches, 8 inches, 10 inches, 12 inches and 14 inches were examined. The 4 inch shadow shield precluded the investigation of shorter distances. In each series all seventeen shells were placed one at a time in position and a ten-minute count was taken. Also a count was taken without a shell to determine the counting rate due to all the factors except shell scatter. In order to determine the reproducibility of the measurements, each series was repeated a second time using exactly the same procedure. Between the initial and repeat measurements each experimental geometry was fully dismantled

and then reassembled, to reveal the extent of error that might be introduced by the technique used in changing shells.

The lead shadow shield was removed for the measurement of the direct radiation rate R_D for two different source-to-detector distances. As was discussed in Section III, B, 1, two such measurements were necessary to determine the effective location of the end of the detector, and once this was established, the source term S' could be found from the direct counting rate.

The measurement periods were short with respect to the half-life of the gamma source so that the counts could be treated as random phenomena. The counting rates R were determined from the relationship

$$R = \frac{m \pm \sqrt{m}}{t}$$

where m is the number of counts recorded in time t and $\frac{\sqrt{m}}{t}$ is the standard deviation in the counting rate.

D. Experimental Results

The discussion of the experimental results is divided into four areas. These are the reproducibility of measurements, the statistical deviations in the final data, the indicated scattering relationships and the shortcomings in the experimental program.

Two measurements were made for each scattering geometry to determine how well each experimental set-up could be reproduced. The results were quite favorable. The difference between the two measured counting rates averaged about 2.7 per cent of their mean value. From this indication of good reproducibility it was concluded that very little error was introduced by the frequent assembly and disassembly of the experimental set-up.

The primary reason that the results of the previous investigation could not be evaluated was the large statistical uncertainty in the experimental data. This problem was effectively eliminated in the present study. The shadow shield removed the large direct radiation component, leaving essentially only scattered activity. The isolation of the experiment in the center of the room reduced the contribution from floor scatter, and the use of a larger source increased the counting rates by a factor of approximately ten. All of these modifications in the procedure had the resultant effect of reducing the standard deviations of the

net counting rates down to the order of two or three counts per minute. The average standard deviation was 8.2 per cent of the net counting rates.

The experimental results for all five series of measurements are tabulated in the Appendix. Two families of curves, Figure 8 and 9, were drawn using the data from Series 2 (h_5 = 8 inches) to illustrate the effect of changes in radius and thickness respectively on the net shell-scattered activity. The solid lines represent experimental findings, the broken lines are plotted from theoretical values.

A third family of curves, Figure 10, was drawn to illustrate the relationship between the five series, each series corresponding to a different source-to-detector distance h_5. The counting rates plotted in this curve were average values of R_S for the four shell thicknesses measured. By this means sixteen curves could be satisfactorily represented by only four composite curves to illustrate the effect of variations in the single parameter, source-to-detector distance. It is seen that the effect of changes in h_5 is less pronounced for the shells of greater radii. Generally, there is a rise in the scattered activity as h_5 decreases, except at the shortest distance, 6 inches, where the counting rate gain becomes less. This decrease is attributed to an idiosyncrasy of the experimental technique. When the shadow shield was positioned very near the detector, the shield

presumably blocked some of the scattered activity coming from the shell wall.

No curves were plotted to show the effect of changes in the shell length h_4 because there was no ostensible effect of variations in this parameter, as seen from the net counting rates listed below for shells of constant radius (3 inches) and thickness (0.064 inches).

Shell length inches	Series 1	Series 2	Series 3	Series 4	Series 5
16	50.6	69.2	67.8	59.7	41.8
24	51.7	67.9	65.6	56.7	47.2
32	50.4	71.6	65.4	57.0	43.8

It should be noted that the entire foregoing discussion of the scattering geometry assumes the detector is positioned above the point source on a vertical axis. The discussion is nonetheless applicable to the present experimental program where the locations of source and detector were reversed.

The major areas of weakness in the experimental program were (1) the inflexibility of the shadow shield, and (2) the anisotropy and energy dependence of the end-window G-M counter. The cone-shaped shield casts a shadow of constant solid angle, whereas, the end of the detector subtends a different solid angle for each value of h_5. Although this

shortcoming is not serious within a limited range of scattering geometries, it would become quite significant for either very small or very large source-to-detector distances. A variety of different cone-shaped shields would provide a solution to this difficulty.

The Geiger counter used was anisotropic both in its counting properties and the solid angle it subtended. A spherical counter with a uniform wall would have essentially eliminated these two difficulties. However, any Geiger-Mueller type detector would still present the problem of the detection efficiency being strongly dependent on the energy of the gamma rays.

V. COMPARISON OF THEORY WITH EXPERIMENT

The experimental data for net shell-scattered activity were compared with the theoretical predictions for these values. (See Figures 8 and 9.) There seemed to be a similarity in the major trends such as a direct increase in counting rate with increasing wall thickness and a decrease in counting rate with increasing shell radius. However, the theoretical analysis did not satisfactorily predict the magnitude of the experimental counting rates. First, the measured values were roughly 23 per cent of the predicted value. (In Figures 8 and 9 a scale factor of 0.25 was used in order to superimpose the curves.) Second, the slopes of the experimental curves are generally smaller than those of the theoretical curves.

The first effect can be attributed to an incorrect determination of one of the constant terms in the coefficient of the theoretical expression. The error is most likely in the source term S. This term was calculated from a measurement of the direct radiation into the covered end-window of the detector. Then, with the assumption that the detection efficiency of the counter was uniform for all incident photons, the same value of S was used to predict the counting rates for the shell scattered activity. This appears to have been a major fallacy. The gamma ray sensitivity of a G-M counter with a low Z cathode, like the one used here,

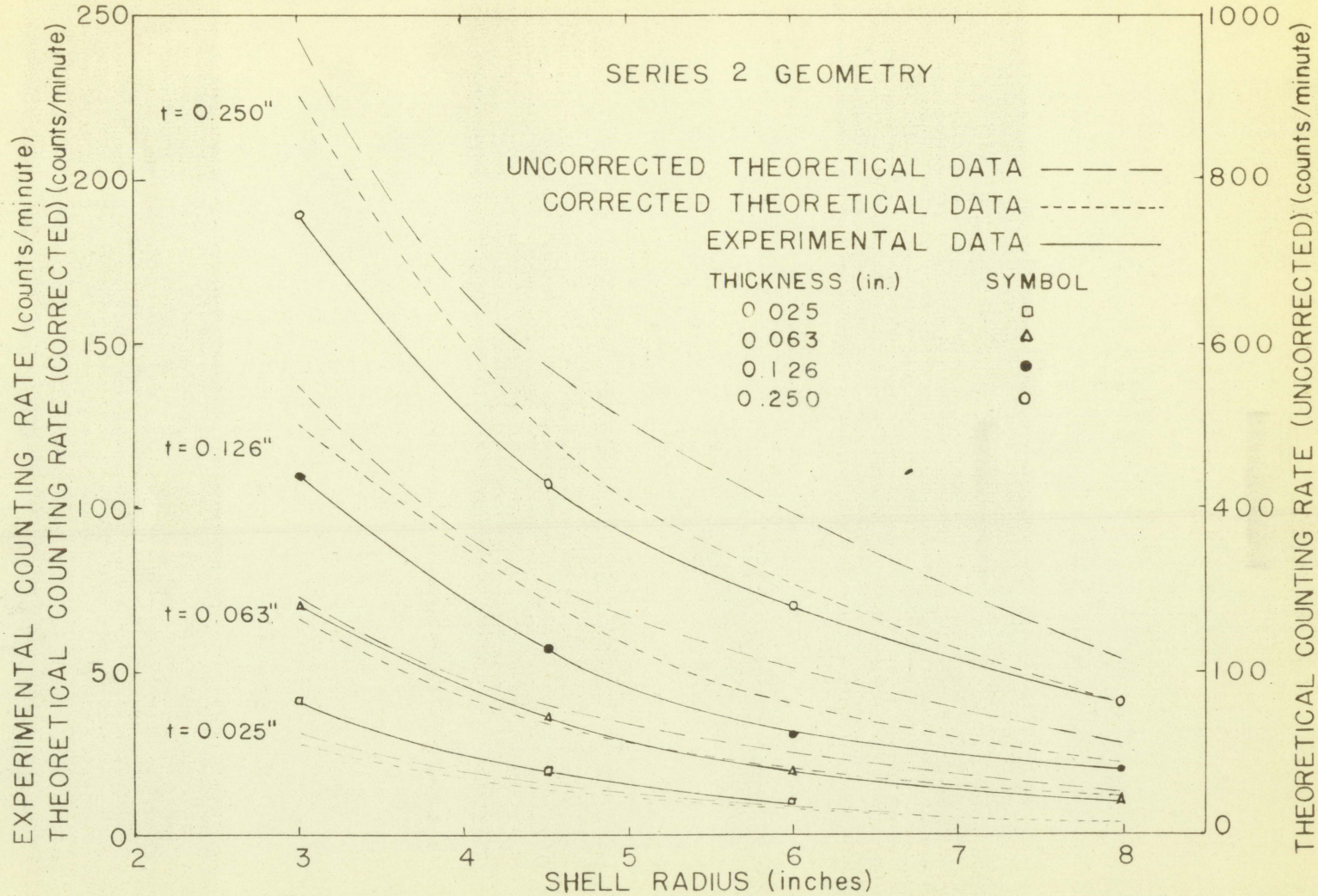

Figure 8. Variation in scattered gamma radiation with shell radius

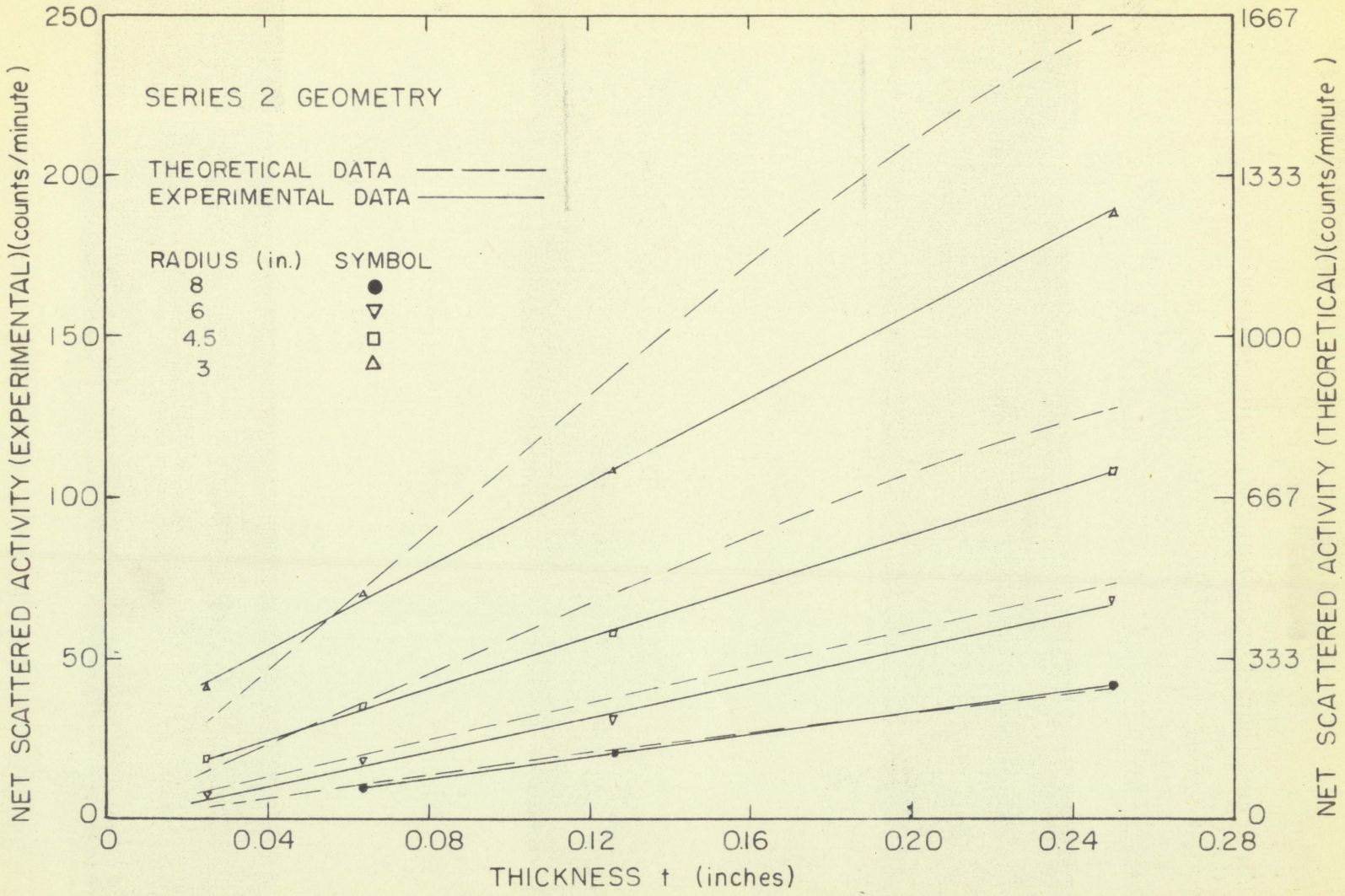

Figure 9. Variation in scattered gamma activity with shell thickness

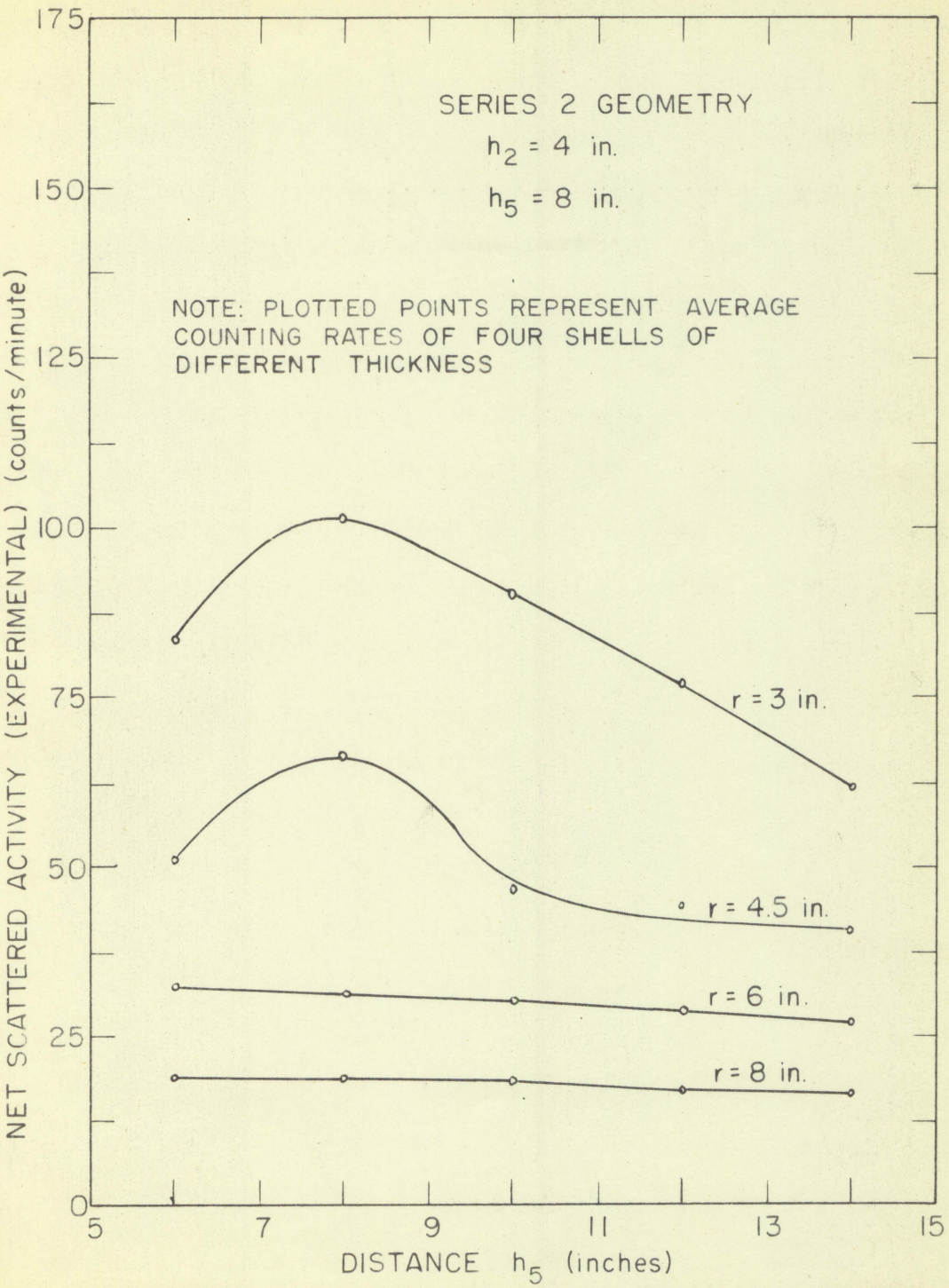

Figure 10. Variation in scattered gamma activity with distance h_5

is roughly proportional to the energy of the photon. This means that the scattered photons with energies on the order of one-fourth of the initial radiation would have about one-fourth of the probability of being detected by the G-M counter. This difficulty might be eliminated in either of two ways. The theoretical expression may be modified to take into consideration the reduced detection sensitivity of the G-M counter for scattered activity or, on the other hand, a scintillation type detector may be employed to avoid the poor detection characteristics inherent in the G-M counter.

Another calculation was made to verify that the energy dependence of the detector was the source of the error in the theory. An additional term, $\frac{a}{a_o}$, expressing the reduced energy and, consequently, the reduced counting efficiency for scattered quanta, was included in the theoretical expression to yield

$$n_s = \frac{S\, n_e\, t}{2} \sum \frac{A}{r_2^2} \frac{d\sigma}{d\Omega} \frac{a}{a_o} e^{-\mu_w(t_1 + t_2)} \frac{\sin^2 \theta}{r} \Delta h \quad .$$

Sample data for this correction are included in the Appendix and the corrected theoretical counting rates are shown in Figure 8 by the dotted curves. It is seen that the corrected theoretical values predict fairly well the experimental data.

The other respect in which the theoretical and experimental curves differ is the smaller slope of the experimental curves. This problem is indicated particularly in Figure 9 where the experimental curves do not seem to converge at the origin as would be expected when the thickness of the scattering material becomes zero. A suggested explanation of this effect is that the net scattered activity from the thicker shells is somewhat less than the analysis predicts. In the analytical treatment the assumption was made that the total absorption coefficient for the wall μ_w was equal for both incident and emerging photons. This is an unsatisfactory assumption since the emerging photons with one-sixth of their original energy have a greater probability for absorption in the shell wall. The absorption coefficient for emerging photons is a different value for each scattering angle, but for large scattering angles the μ_w for emerging gamma rays is approximately 0.3 cm^{-1}, as compared to 0.15 cm^{-1} for photons with 1.25-Mev initial energy. A correction in the absorption coefficient for the emerging photons would result in lower predicted values of scattered activity from the thicker shells.

There appears to be one unaccounted for difficulty in this explanation. The experimental data plotted in Figure 9 seem to fall on straight line curves indicating a linear dependence of scattering activity on the wall thickness. However, the proposed absorption correction would introduce

another exponential term that would only increase the tendency toward "bending" that already appears in the theoretical curves. Although the increase in the wall absorption term seems to be a sound application of principle, it does not properly account for the shape of the experimental curves.

The lack of significant variation in scattered activity with an increase in shell length is relatively easy to explain. Not all portions of the shell length contribute equally to the activity scattered into the detector. As indicated in Figure 6, the portion of the shell wall which lies near the detector is expected to make the largest contribution to the counting rates. Conversely, the opposite end of the shell, beyond the source, contributes very little. In the experimental work the 24 and 32 inch shells extended beyond the source 8 and 16 inches respectively into a region where their contributions to the detected activity were quite small. The region of minimum scattering contribution was found in the analysis to fall directly opposite the detector for shells of very small radius, and midway between the source and detector for shells of very large radius.

VI. CONCLUSIONS

The major difficulties of the study seemed to be related to the particular detection device employed, the end-window G-M counter. Its cylindrical shape caused a complicated problem of solid angle; its non-uniform walls resulted in anisotropic detection characteristics; and its strong energy dependence, characteristic of G-M counters, introduced a problem of variable sensitivity for the poly-energetic, scattered photons.

A possible area for further investigation lies in the use of a NaI crystal in connection with a photomultiplier tube. Although complete isotropy of solid angle and of sensitivity may be difficult to achieve, due to the "shadow" of the P-M tube, these objectives could be approached. The primary advantages, however, would be the high detection efficiency and the capability of detecting gamma rays in a wide range of energies. With this type of detector and scaling equipment with energy "gates" the energy spectrum of the scattered activity as a function of the scattering region in the shell wall could be investigated as a further extension of the present problem.

Although the original theoretical expression did not predict the values of the net shell-scattered counting rates within a factor of four, there was a reasonable similarity between the findings from theory and experiment.

The error in the theory was attributed to the neglect of the non-uniform counter efficiency for scattered photons. This difficulty seems to be eliminated by the inclusion in the theoretical equation of another variable term to account for the variation in energy of the scattered radiation.

VII. LITERATURE CITED

1. Ney, Kenneth C. Similitude considerations in neutron and gamma ray scattering. Unpublished M.S. Thesis. Ames, Iowa, Iowa State College Library. 1955.

2. Plesset, M. S. and Cohen, S. T. Scattering and absorption of gamma-rays. Journal of Applied Physics. 22: 350-357. 1951.

3. Latter, Richard and Kahn, Herman. Gamma-ray absorption coefficients. Rand Corporation Report R-170. 1949.

4. Alcoa aluminum and its alloys. Pittsburg, Pa., Aluminum Company of America. 1947.

VIII. ACKNOWLEDGMENTS

The author wishes to express his appreciation to Dr. Glenn Murphy of the Department of Theoretical and Applied Mechanics for the original suggestion of this problem and also for the guidance and assistance which he gave during this investigation.

The author would like to thank the Engineering Experiment Station of Iowa State College for the equipment and facilities made available for the experimental portion of this study. The investigation reported in this thesis was conducted as a project in the Iowa Engineering Experiment Station.

IX. APPENDIX

Table 3

Experimental data for measurement series 5

Shell dimensions			Run 1		Run 2		Average
r (in.)	h_4 (in.)	t (in.)	Counting rate (R) (counts per minute)	Net rate (R_S) (counts per minute)	Counting rate (R) (counts per minute)	Net rate (R_S) (counts per minute)	Net counting rate (counts per minute)
	none		37.2	-	38.8	-	38.0 ± 1.9
3	16	0.025	70.6	33.4	70.9	32.1	32.8 ± 2.3
4.5	16	0.025	56.3	19.1	57.5	18.7	18.9 ± 2.2
6	16	0.025	51.4	14.2	50.1	11.3	12.8 ± 2.1
3	16	0.063	79.6	42.4	80.0	41.2	41.8 ± 2.4
3	24	0.063	88.2	51.0	82.3	43.5	47.2 ± 2.5
3	32	0.063	82.3	45.1	82.6	43.8	44.5 ± 2.5
4.5	16	0.064	66.5	29.2	70.5	31.7	30.5 ± 2.3
6	16	0.064	57.4	20.2	57.6	18.8	19.5 ± 2.2
8	16	0.064	50.6	13.4	49.5	10.7	12.0 ± 2.1
3	16	0.126	102.8	65.6	108.8	70.0	68.7 ± 2.7
4.5	16	0.126	79.6	42.4	84.1	45.3	43.8 ± 2.5
6	16	0.126	64.5	27.3	65.1	26.3	26.8 ± 2.3
8	16	0.126	53.2	16.0	53.6	14.8	15.4 ± 2.1
3	16	0.250	145.9	108.7	142.2	103.4	106.1 ± 3.0
4.5	16	0.250	107.6	70.4	108.1	69.3	69.9 ± 2.7
6	16	0.250	84.8	47.6	87.6	48.8	48.4 ± 2.5
8	16	0.250	71.5	34.3	70.3	31.5	32.9 ± 2.3

Table 4

Experimental net counting rates for shell-scattered gamma activity

Shell dimensions			Series 1	Series 2	Series 3	Series 4	Series 5
r (in.)	h_4 (in.)	t (in.)	Counting rate (counts per minute)	Counting rate (counts per minute)	Counting rate (counts per minute)	Counting rate (counts per minute)	Counting rate (counts per minute
3	16	0.025	23.1 ± 2.4	41.7 ± 2.6	44.3 ± 2.4	36.2 ± 2.4	32.8 ± 2.3
4.5	16	0.025	13.0 ± 2.3	18.0 ± 2.4	17.8 ± 2.1	21.5 ± 2.3	18.9 ± 2.2
6	16	0.026	10.8 ± 2.2	8.9 ± 2.3	11.5 ± 2.0	11.7 ± 2.2	12.8 ± 2.1
3	16	0.063	50.6 ± 2.7	69.2 ± 2.9	67.8 ± 2.6	59.7 ± 2.7	41.8 ± 2.4
3	24	0.063	51.7 ± 2.7	67.9 ± 2.9	65.6 ± 2.6	56.7 ± 2.6	47.2 ± 2.5
3	32	0.063	50.4 ± 2.7	71.6 ± 2.9	65.4 ± 2.6	57.0 ± 2.7	44.5 ± 2.5
4.5	16	0.064	25.4 ± 2.4	34.9 ± 2.6	29.0 ± 2.2	27.1 ± 2.4	30.5 ± 2.3
6	16	0.064	17.3 ± 2.3	18.0 ± 2.4	16.9 ± 2.1	18.9 ± 2.3	19.5 ± 2.2
8	16	0.064	10.6 ± 2.2	10.6 ± 2.3	13.0 ± 2.0	11.4 ± 2.2	12.0 ± 2.1
3	16	0.126	85.9 ± 3.0	107.8 ± 3.1	91.0 ± 2.8	82.2 ± 2.9	67.8 ± 2.7
4.5	16	0.126	57.6 ± 2.7	56.6 ± 2.8	48.6 ± 2.4	48.3 ± 2.6	43.8 ± 2.5
6	16	0.126	34.2 ± 2.5	29.7 ± 2.5	34.3 ± 2.2	31.3 ± 2.4	26.8 ± 2.3
8	16	0.126	19.1 ± 2.3	19.6 ± 2.4	18.5 ± 2.1	16.1 ± 2.2	15.4 ± 2.1
3	16	0.250	173.4 ± 3.6	187.0 ± 3.8	158.9 ± 3.4	129.6 ± 3.3	106.1 ± 3.0
4.5	16	0.250	107.7 ± 3.1	106.5 ± 3.2	90.0 ± 2.8	80.2 ± 2.9	69.9 ± 2.7
6	16	0.250	67.4 ± 2.8	68.1 ± 2.9	57.9 ± 2.5	51.9 ± 2.6	48.4 ± 2.5
8	16	0.250	43.0 ± 2.6	40.4 ± 2.6	35.0 ± 2.3	34.0 ± 2.4	32.9 ± 2.3

Table 5

Computed data for graphical solution of theoretical equation for series 2 geometry (r = 4.5 inches, t = 0.063 inches, h_4 = 16 inches, h_5 = 8 inches)

h	r_2^2	$\sin^2\theta$	$\frac{d\sigma}{d\Omega}$	$e^{-\mu_w(t_1+t_2)}$	A	$\frac{a}{a_o}$	$\frac{A}{r_2^2}\frac{d\sigma}{d\Omega}\frac{\sin^2\theta}{r}e^{-\mu_w(t_1+t_2)}$	
			cm^2 per electron steradian				cm^2 per electron per inch	
(in.)	(in.^{2})	(in.$^{-1}$)	x 10^{-26}		(in.^{2})		x 10^{-29} (uncorrected)	x 10^{-30} (corrected for $\frac{a}{a_o}$)
0	36.25	0.123	.707	.951	2.104	.1785	1.068	1.905
1	29.25	0.143	.712	.955	2.122	.1830	1.570	2.87
2	24.25	0.168	.721	.959	2.225	.1898	2.37	4.49
3	21.25	0.198	.735	.962	2.181	.207	3.19	6.62
4	20.25	0.240	.758	.964	2.363	.215	4.55	9.78
5	21.25	0.291	.789	.966	2.181	.233	5.07	11.80
6	24.25	0.358	.824	.967	2.225	.250	5.81	14.52
7	29.25	0.449	.853	.968	2.122	.263	5.98	15.73
8	36.25	0.558	.866	.968	2.104	.268	6.04	16.18
9	45.25	0.692	.953	.968	2.020	.263	5.67	14.90
10	56.25	0.833	.824	.967	1.932	.250	5.07	12.68
11	69.25	0.951	.789	.966	1.850	.233	4.31	10.02
12	84.25	0.997	.758	.964	1.774	.215	3.40	7.32
13	101.25	0.951	.735	.962	1.709	.207	2.52	5.22
14	120.25	0.833	.721	.959	1.648	.1898	1.755	3.33
15	141.25	0.692	.712	.955	1.596	.1830	1.180	2.16
16	164.25	0.558	.707	.951	1.585	.1785	0.807	1.44